Current trends and future challenges in the experimental, theoretical and computational analysis of intervalence charge transfer (IVCT) transitions

Deanna M. D'Alessandro and F. Richard Keene*

Mixed-valence chemistry has a long and rich history which is characterised by a strong interplay of experimental, theoretical and computational studies. The intervalence charge transfer (IVCT) transitions generated in dinuclear mixed-valence species (particularly of ruthenium and osmium) have received considerable attention in this context, as they provide a powerful and sensitive probe of the factors which govern electronic delocalisation and the activation barrier to intramolecular electron transfer. This *tutorial review* discusses classical, semi-classical and quantum mechanical theoretical treatments which have been developed over the past 35 years for the analysis of IVCT absorption bands. Particular attention is drawn to the applicability of these models for the analysis of mixed-valence complexes which lie between the fully localised (Class II) and delocalised (Class III) limits in the ''localised-to-delocalised'' (Class II–III) regime. A clear understanding of the complex interplay of inter- and intramolecular factors which influence the IVCT process is crucial for the design of experimental studies to probe the localised-to-delocalised regime and in guidance of the development of appropriate theoretical models.

1. Introduction

Electron transfer is ubiquitous in chemical, physical and biological systems. Its importance underlies the extensive multidisciplinary research efforts into mixed-valence species; in particular, dinuclear mixed-valence complexes have received significant attention in this context as the characteristics of their intervalence charge transfer (IVCT) absorption bands—specifically,

School of Pharmacy and Molecular Sciences, James Cook University, Townsville, Queensland 4811, Australia.
E-mail: Richard.Keene@jcu.edu.au; Fax: +61-(0)7-4781-6078

their energy (v_{max}), intensity (ε) and bandwidth at half-height ($\Delta v_{1/2}$)—provide a powerful and sensitive probe for elucidating the fundamental factors that govern intermolecular electron transfer reactions in natural and artificial systems. In the late 1960's, Hush provided a theoretical model linking the parameters of their IVCT bands to the activation barriers for electron transfer derived from Marcus theory, as shown in eqn (1).[1]

$$v_{max} = hv = \lambda_i + \lambda_o + \Delta E_0 + \Delta E'$$ (1)

The Franck–Condon factors (λ_i and λ_o) correspond to the reorganisational energies within the inner- and outer-sphere,

Deanna M. D'Alessandro

Deanna obtained her BSc specialising in chemistry, physics and mathematics at James Cook University, and received the University Medal in 2000 following Honours studies in chemistry. She has recently completed her PhD (awarded cum laude) under the supervision of Professor Richard Keene, in which she studied the design and synthesis of stereochemically-unambiguous polymetallic assemblies and the elucidation of spatial effects on their electron transfer properties. During her postgraduate studies, she has been the recipient of two awards for her research at national conferences, including a Don Stranks Award of the Royal Australian Chemical Institute in 2003.

F. Richard Keene

Richard Keene graduated from the University of Adelaide, and subsequently undertook postdoctoral work at the Australian National University and the University of North Carolina at Chapel Hill. On his return to Australia he was appointed to James Cook University in Townsville, where he is now the Nevitt Professor of Chemistry. He is a recipient of the Rennie Medal of the Royal Australian Chemical Institute. Richard has published in a number of areas of coordination chemistry, but his present research interests relate primarily to the stereochemistry of metallosupramolecular assemblies and its effect on their physical properties—in particular intramolecular electron transfer, and their interaction with biological molecules such as DNA.

respectively, the redox asymmetry (ΔE_0) is the energy difference between the vibrationally-relaxed initial and final states in the hypothetical absence of electronic coupling, and $\Delta E'$ reflects any additional energy contributions due to spin–orbit coupling and ligand field asymmetry.

The mixed-valence forms of ligand-bridged dinuclear polypyridyl complexes of ruthenium and osmium have played a crucial role in the assessment of activation barriers to intramolecular electron transfer since the disclosure of the Creutz–Taube ion, $[\{Ru(NH_3)_5\}(\mu\text{-pyz})\{Ru(NH_3)_5\}]^{5+}$ (pyz = pyrazine), in 1973.[2] A pivotal issue in the analysis of mixed-valence complexes is the extent of electronic coupling between the metal centres, and the classification of the mixed-valence systems as localised (Class II) or delocalised (Class III).[3] While clear examples of localised and delocalised systems have been reported in several comprehensive surveys of dinuclear mixed-valence complexes,[4–11] a number of recent reports have highlighted systems which exhibit intermediate behaviour in the localised-to-delocalised (Class II–III) regime.[12–14] In reality, the transitions between regimes are not abrupt, and experimental studies have revealed a gradation in behaviour between the fully localised and fully delocalised limits which is governed by the relative timescales for intramolecular electron transfer and multiple nuclear and solvent vibrations which are coupled to the electron transfer.[12] The description is further challenged experimentally by the appearance of multiple IVCT bands in transition metal-containing chromophores, in addition to contributions from environmental effects such as specific solvation and ion-pairing which are not explicitly included in theoretical treatments for IVCT.[11]

While classical models are the preferred method of analysis of IVCT bands due to the facility of their application, the classical approach is strictly valid in the limits of strong localisation and delocalisation only. For this reason, the development of a theoretical framework which provides a coherent and physically transparent basis for the treatment of mixed-valence systems between these limits represents an important thrust of current research in the field.

In the present review, we draw attention to the multitude of intra- and intermolecular effects which influence IVCT, and consider experimental, theoretical and computational approaches which have probed their contributions to the activation barrier for intramolecular electron transfer. The

understanding of the subtle interplay of factors which determine the nature of IVCT transitions is crucial for meaningful comparisons between IVCT data, and if the implications of the results are to be fully realised at both a fundamental and applied level.

2. Theoretical background

2.1 Two-state classical and semi-classical theories of IVCT

The IVCT transition in dinuclear mixed-valence species may be examined by considering a complex of the type $[\{M_1(L)_n\}(\mu\text{-BL})\{M_2(L)_n\}]^{4+}$ (where M_1 and M_2 represent the metal centres; L and BL represent the terminal and bridging ligands respectively), hereafter abbreviated $[M_1^{II}M_2^{II}]$, where both metal centres are in the +II oxidation state. The oxidation of one metal centre gives rise to the mixed-valence species, where the overall +5 charge corresponds to $[M_1^{II}M_2^{III}]$ in a fully localised description and $[M_1^{II1/2}M_2^{II1/2}]$ in a fully delocalised description.[1] A symmetrical dinuclear complex is typically described by the parabolic potential energy surfaces depicted in Fig. 1, where the dimensionless reaction coordinate (X) represents an anti-symmetric combination of the metal–ligand and solvent stretching vibrations. The dotted curves correspond to the wavefunctions Ψ_a and Ψ_b for the valence-localised electronic isomers $[M_1^{II}M_2^{II}]_0$ and $[M_1^{III}M_2^{II}]_0$, respectively, where the odd electron is completely localised on either metal centre. These diabatic states are centred at $X_{min} = 0$ and 1 on the reaction coordinate and are assumed to be harmonic with identical force constants. Their energies are given by H_a and H_b in eqn (2), where $\hat{H}$ is the effective two-state Hamiltonian operator and λ is the reorganisational energy.

$$H_a = \langle\Psi_a|\hat{H}|\Psi_a\rangle = \lambda X^2 \text{ and} \\ H_b = \langle\Psi_b|\hat{H}|\Psi_b\rangle = \lambda(X-1)^2 \tag{2}$$

At the intersection of the diabatic surfaces ($X = 0.5$), the mixing between the wavefunctions removes the degeneracy and gives rise to two new adiabatic surfaces, depicted by the solid curves in Fig. 1(b). The energies of the lower and upper adiabatic states, E_- and E_+ (respectively), are given by eqn (3),[15] and the splitting between the surfaces at $X = 0.5$ defines the electronic coupling parameter, $H_{ab} = \langle\Psi_a|\hat{H}|\Psi_b\rangle$.
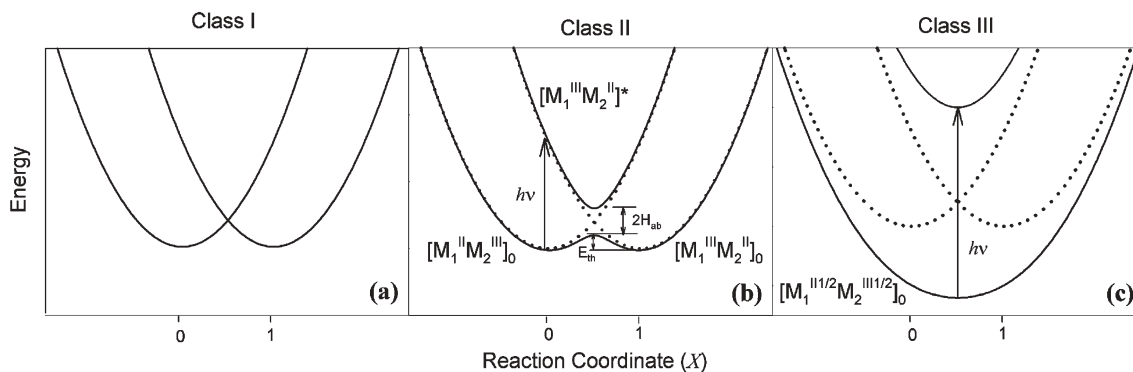
Fig. 1 Potential energy curves for electron transfer in ligand-bridged dinuclear complexes with (a) negligible, (b) weak ($H_{ab} = \lambda/4$) and (c) strong ($H_{ab} = 3\lambda/4$) electronic coupling. The dotted and solid curves represent the diabatic and adiabatic surfaces, respectively.

This journal is © The Royal Society of Chemistry 2006

Chem. Soc. Rev., 2006, **35**, 424–440 | 425

$$E_\pm = \frac{\left[\lambda(2X^2 - 2X + 1)\right]}{2} - \frac{\left\{[\lambda(2X - 1)]^2 + 4H_{ab}^2\right\}^{1/2}}{2} \quad (3)$$

The optically-induced vertical transition between the adiabatic states is the IVCT transition {eqn (4)}, which corresponds to the formation of the vibrationally excited state of the ion, $[M_1^{III}M_2^{II}]^*$. Since this process proceeds faster than nuclear motion (in accordance with the Franck–Condon Principle), $[M_1^{III}M_2^{II}]^*$ contains $[M_1^{III}]^*$ in a coordination environment appropriate for $[M_1^{II}]_0$, and $[M_2^{II}]^*$ in a coordination environment appropriate for $[M_2^{III}]_0$.

$$\left[M_1^{II}M_2^{III}\right]_0 \xrightarrow{h\nu} \left[M_1^{III}M_2^{II}\right]^* \quad (4)$$
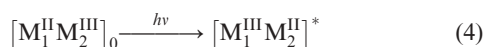
The degree of electronic coupling between M_1 and M_2, and the resultant splitting between the adiabatic surfaces, dictate the class of a mixed-valence system within the Robin and Day classification scheme.[3] When M_1 and M_2 are far apart or when their interaction is symmetry or spin forbidden, the electronic coupling is negligible ($H_{ab} = 0$) and IVCT transitions are not possible. This situation is illustrated in Fig. 1(a) and corresponds to Class I.[3] Class II systems are characterised by weak to moderate electronic coupling between M_1 and M_2, and exhibit IVCT bands due to the vertical transition between the adiabatic states at X_{min} {Fig. 1(b)}. As H_{ab} increases, the greater vertical splitting between the adiabatic surfaces is compensated for by the reactant and product minima moving closer together such that the energy of the transition ($h\nu$) is equal to λ within the Class II regime according to eqn (5) {where $\lambda = \lambda_i + \lambda_o$; ΔE_0 and $\Delta E' = 0$ in eqn (1)}.[14,15] While λ is a property of the diabatic states and corresponds to the transfer of unit charge, the adiabatic reorganisational energy, λ', corresponds to the actual charge transferred, as expressed in eqn (6). λ' is reduced relative to λ by delocalisation, and vanishes when $\lambda = 2H_{ab}$.

$$h\nu = \lambda = \lambda' + 4H_{ab}^2/\lambda \quad (5)$$

$$\lambda' = \lambda(1 - 4H_{ab}^2/\lambda^2) \quad (6)$$

In addition to the optically-activated IVCT process, electron transfer can occur by thermal activation and surface crossing on the ground state adiabatic surface in Fig. 1(b). The energies of the thermal and optical processes are directly related,[1] and the energetic barrier for thermal electron transfer,[14,15] E_{th}, is given by eqn (7).

$$E_{th} = \lambda/4 - H_{ab} + H_{ab}^2/\lambda \quad (7)$$

Within the Class II regime, the IVCT bands are typically weak ($\varepsilon_{max} \leqslant 5000$ M^{-1}cm^{-1}), solvent-dependent, and exhibit large bandwidths ($\Delta\nu_{1/2} \geqslant 2000$ cm^{-1}). In the two-state limit, the predicted bandwidth, $\Delta\nu_{1/2}°$, is given by eqn (8), where R is the gas constant, T is the temperature (in K), and the term $16RTln2$ takes a value of 2310 cm^{-1} at 298 K.

$$\Delta\nu_{1/2}° = [16RTln2(\lambda)]^{1/2} = \\ [16RTln2(\nu_{max} - \Delta E_0 - \Delta E')]^{1/2} \quad (8)$$

For Gaussian-shaped IVCT bands, H_{ab} is given by eqn (9),[1] where r_{ab} is the distance between the two diabatic states. A more rigorous quantum mechanical formulation is given by eqn (10),[14] where $|\mu_{12}|$ is the adiabatic transition dipole moment and e is the unit electronic charge. This form of the equation for H_{ab} has the advantage that no implicit assumption is made regarding the shape of the IVCT band, as $|\mu_{12}|$ may be calculated from the integrated intensity of the absorption band.

$$H_{ab} = \frac{2.06 \times 10^{-2}\left(\nu_{max}\varepsilon_{max}\Delta\nu_{1/2}\right)^{1/2}}{r_{ab}} \quad (9)$$

$$H_{ab} = \frac{|\mu_{12}|}{er_{ab}}\nu_{max} \quad (10)$$

The above-mentioned classes of mixed-valence systems are distinguished by the relative magnitudes of λ and $2H_{ab}$. For weakly-coupled Class II systems, $2H_{ab} \ll \lambda$. When M_1 and M_2 are strongly electronically coupled ($2H_{ab} \gg \lambda$), the thermal barrier to intramolecular electron transfer vanishes and the ground state adiabatic surface exhibits a single minimum at $X_{min} = 0.5$ {Fig. 1(c)}. In these delocalised Class III systems, both metal centres possess a partial oxidation state of +II½ and the IVCT transitions occur within the molecular orbital manifolds of the systems. While the terms "IVCT transition" and "mixed-valence" are retained, the transitions do not involve net charge transfer and the systems are more accurately defined as "average valence". The transitions are typically intense ($\varepsilon_{max} \geqslant 5000$ M^{-1}cm^{-1}), solvent-independent and exhibit narrow bandwidths ($\Delta\nu_{1/2} \leqslant 2000$ cm^{-1}). The energies of the IVCT bands provide a direct measure of H_{ab} since $H_{ab} = $ ½ν_{max}.[1]

2.2 The reorganisational energy

The reorganisational energy, λ, is partitioned into two independent contributions corresponding to the inner- (λ_i) and outer-sphere (λ_o) reorganisational energies.[1] λ_i represents the energy required for reorganisation of the metal–ligand and intra-ligand bond lengths and angles, and λ_o is the energy required for reorganisation of the surrounding solvent medium. Classical expressions for λ_i are formulated in terms of the equilibrium bond length changes and force constants of the reactants and products, but are appropriate for low frequency modes which are coupled to the electron transfer, such as vibrations in polar solvents. However, the model is inadequate for systems which exhibit coupled high-frequency quantum modes[16] which may be evaluated experimentally by resonance Raman spectroscopy,[17] and treated through a quantum mechanical approach.[8]

The λ_o contribution is generally treated as a one-dimensional classical mode due to the low frequencies of coupled solvent vibrations.[1] According to the spherical cavity dielectric continuum model given in eqn (11), the solvent is treated as a structureless dielectric continuum and has no specific interactions with itself or with the redox sites.[1] The two metal centres of a symmetrical dinuclear complex are assumed to be centrally located in two non-interpenetrating spheres

$(d \gg 2a)$ embedded in the dielectric. The parameters a and d define the molecular radii and distance between the donor and acceptor, and D_s and D_{op} are the static and optical dielectric constants of the solvent, respectively.

$$\lambda_o = e^2 \left(\frac{1}{a} - \frac{1}{d} \right) \left(\frac{1}{D_{op}} - \frac{1}{D_s} \right) \qquad (11)$$

In accordance with eqn (1) and (11), ν_{max} should vary linearly with the solvent dielectric function $(1/D_{op} - 1/D_s)$, with slope $e^2(1/a - 1/d)$ and intercept $\lambda_i + \Delta E'$. The validity of the dielectric continuum model is typically assessed experimentally through IVCT solvatochromism measurements.[1,4,6,7,12] The sensitivity of IVCT bands to solvent variation is often employed as a criterion for the class of a mixed-valence species: a solvent dependence signals valence localisation (Class II), while a solvent independence signals delocalisation (Class III).

It must be noted that eqn (11) neglects the volume occupied by the donor and acceptor (the excluded volume) and is valid only when the distance between the redox centres exceeds the sum of their radii $(d \gg 2a)$. The corrections due to interpenetrating spheres and non-spherical fields around the metal centres become increasingly important as the distance between the metal centres is decreased.

3. The analysis of IVCT transitions according to two-state classical and semi-classical models

3.1 The extent of electronic coupling

3.1.1 Spectral methods. The classification of mixed-valence complexes is dependent on the relative magnitudes of λ and H_{ab}; however, this criterion is often complicated by the inability to accurately determine H_{ab}. While r_{ab} is typically equated with the through-space geometrical distance between the metal centres in eqn (9) and (10), the *effective* charge transfer distance may be shorter due to electronic delocalisation, self-polarisation and other effects, so that the equations provide a lower limit only for H_{ab}.[12] In addition, band-shape analyses are frequently complicated by the presence of multiple overlapping IVCT and interconfigurational (IC) transitions which arise from the effects of low symmetry and spin–orbit coupling in transition metal complexes.[12] These issues are the subjects of §5.2.2 and §5.2.5.

While the Hush model[1] is the preferred method of analysis for IVCT bands, alternate spectral methods for extracting the electronic coupling parameter have been sought which do not rely primarily on the characteristics of the bands. The "CNS" approach introduced by Creutz, Newton and Sutin is based upon a superexchange formalism (§5.2.1), in which the metal–metal coupling is facilitated by mixing with a metal-to-bridging ligand charge transfer (MLCT) and/or bridging ligand-to-metal charge transfer (LMCT) state.[15,18] For a dinuclear system M_1-BL-M_2, the electronic coupling parameter (denoted by $H_{M_1M_2}$ instead of H_{ab}) may be calculated from eqn (12a).

$$H_{M_1M_2} = \frac{H_{M_1L}H_{M_2L}}{2\Delta E_{ML}} + \frac{H_{LM_1}H_{LM_2}}{\Delta E_{LM}} \qquad (12a)$$

$$\frac{1}{\Delta E_{ML}} = \frac{1}{2} \left(\frac{1}{\Delta E_{MLCT}} - \frac{1}{\Delta E_{IVCT}} \right) \qquad (12b)$$

Here, H_{M_1L} is the M_1-BL coupling for the M_1^{II} site {determined from the characteristics of the MLCT band by an expression analogous to eqn (9)}, H_{M_2L} is the corresponding quantity for an M_2^{II} site at the M_2^{III} geometry, and ΔE_{M_1L} is the effective M_1-BL energy gap. The latter is determined from eqn (12b), where ΔE_{MLCT} and ΔE_{IVCT} are the energies of the MLCT and IVCT transitions, respectively. The quantities denoted by the subscripts LM_1 and LM_2 are the corresponding values for the LMCT transition. Typically, the coupling of the metal centres is dominated by either an electron or hole transfer superexchange mechanism (see §5.2.1), and eqn (12a) is reduced to the first or second term only. The equations are further simplified by assuming that the quantities denoted by the subscripts M_1L and LM_1 are equivalent to those denoted by M_2L and LM_2, respectively, which is reasonable given the small differences in geometry between the two redox sites. Indeed, for weakly-coupled systems such as $[\{Ru^{II}(NH_3)_5\}(\mu\text{-}4,4'\text{-bpy})\{Ru^{III}(NH_3)_5\}]^{5+}$, the value of the electronic coupling parameter obtained from eqn (9) ($H_{ab} = 900$ cm^{-1}) is in satisfactory agreement with the value calculated from eqn (12a) and (12b) (*i.e.* $H_{M_1M_2} = 800$ cm^{-1}, where $H_{M_1L} = H_{M_2L} = 4.4 \times 10^3$ cm^{-1} and $\Delta E_{M_1L} = 12.7 \times 10^3$ cm^{-1}).[15,18] For a number of Class II systems, the magnitudes of the electronic coupling parameters calculated from the Hush and CNS methods were in close agreement.[9,13] The validity of the CNS method has been questioned due to the need for empirical parameterisation and assumptions regarding the charge transfer distance, a single orbital interaction directed along the M_1–BL–M_2 axis, and the treatment of a single MLCT or LMCT excited state only.[9,13,18]

3.1.2 Electrochemical methods and the comproportionation equilibrium. The comproportionation constant, K_c, and the free energy of comproportionation, ΔG_c° provide alternate measures for determining the degree of electronic delocalisation.[4,19] In the absence of electronic coupling, the two metal centres in a symmetrical dinuclear complex undergo oxidation at approximately the same potential; however, any electronic interaction between the centres leads to the existence of discrete oxidation waves.[4,6,7] In the potential domain between these two processes the complex is in the mixed-valence state, $[M^{II}M^{III}]$. The K_c values for the comproportionation equilibrium express the stability of the $[M^{II}M^{III}]$ species relative to the fully-reduced, $[M^{II}M^{II}]$, and fully-oxidised, $[M^{III}M^{III}]$, forms:

$$\left[M^{II}M^{II}\right] + \left[M^{III}M^{III}\right] \xrightleftharpoons{K_c} 2\left[M^{II}M^{III}\right]$$

$$\text{where,} \quad K_c = \frac{\left[M^{II}M^{III}\right]^2}{\left[M^{II}M^{II}\right]\left[M^{III}M^{III}\right]} \qquad (13)$$
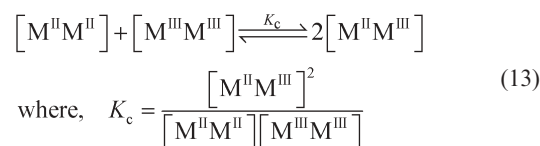
K_c can be measured spectrally or electrochemically from the separation between the two redox potentials for the successive oxidation processes (ΔE_{ox}) according to eqn (14a), where F/RT takes the value 38.92 V^{-1} at 298 K (F is the Faraday constant).[4,19] Large values of K_c and ΔE_{ox} are essential

This journal is © The Royal Society of Chemistry 2006

Chem. Soc. Rev., 2006, **35**, 424–440 | 427

requirements for the isolation of a complex in its mixed-valence state.

$$K_c = \exp(\Delta E_{ox}F/RT) \tag{14a}$$

$$\Delta G_c^\circ = -RT\ln K_c = -\Delta E_{ox}F \tag{14b}$$

Four factors contribute to the magnitude of ΔG_c° {eqn (14b)}: a statistical contribution ($\frac{1}{2}RT\ln\frac{1}{4}$); an electrostatic factor (ΔG_e°) arising from the repulsion of the two similarly charged metal centres linked by the bridging ligand; a synergistic factor (ΔG_s°) due to metal–ligand backbonding interactions; and a resonance stabilisation factor (ΔG_r°) due to electronic delocalisation.[4,19] For localised mixed-valence systems, the first three contributions can be readily estimated.[4,6,7,19] ΔG_r° is the only component that represents the actual metal–metal coupling, and is related to H_{ab} by eqn (15a) and (15b) for localised and delocalised systems, respectively.[15]

$$-\Delta G_r^\circ = 2H_{ab}^2/\lambda = 2H_{ab}^2/\nu_{max} \tag{15a}$$

$$-\Delta G_r^\circ = 2(H_{ab} - \lambda/4) = \nu_{max} - \lambda/2 \tag{15b}$$

The comparison of ΔE_{ox} and K_c values determined from electrochemical data have been widely used for the assessment of the extent of coupling in mixed-valence complexes.[4,6,7,20] However, the comparison between the electronic coupling parameters derived from the semi-classical Hush model,[1] the CNS model,[15,18] and the electrochemical treatment, are frequently in poor agreement.[13] Previous reports have emphasised the need for caution in the interpretation of electrochemical data, due to the significant dependence of redox potentials on the identity of the solvent and anions in the electrolyte medium.[9] Spectral measurements of the IVCT transitions often serve as a more subtle and accurate probe for the degree of electronic coupling.[1]

3.2 Predictions for the IVCT band-shape

The shift between the localised and delocalised regimes is driven by an increase in H_{ab}. The predicted effect of increasing delocalisation on the IVCT band-shape for a symmetrical dinuclear mixed-valence complex is illustrated in Fig. 2.[14] The band is calculated by assuming a Boltzmann distribution over the energies on the ground state adiabatic surface.[1] For $2H_{ab} \ll \lambda$, this produces a Gaussian-shaped contour that is symmetrical about ν_{max}, with a bandwidth of $\Delta\nu_{1/2}^\circ$ {Fig. 2(a) and (b)}. Since wavelength-dependent charge transfer intensities scale with the inverse of the absolute absorption energy (ν^{-1}),[1a] the energy maximum of the "reduced" absorption spectrum (i.e. ε/ν versus ν) is identified by the vertical separation between the lower and upper surfaces, and is the quantity most appropriately employed in the analysis of IVCT bands. As H_{ab} increases, the Gaussian shape is retained, but the band is truncated on the low energy side below $2H_{ab}$, i.e. the minimum difference between the ground and excited states at $X = 0.5$, as shown in Fig. 2(c).[13]
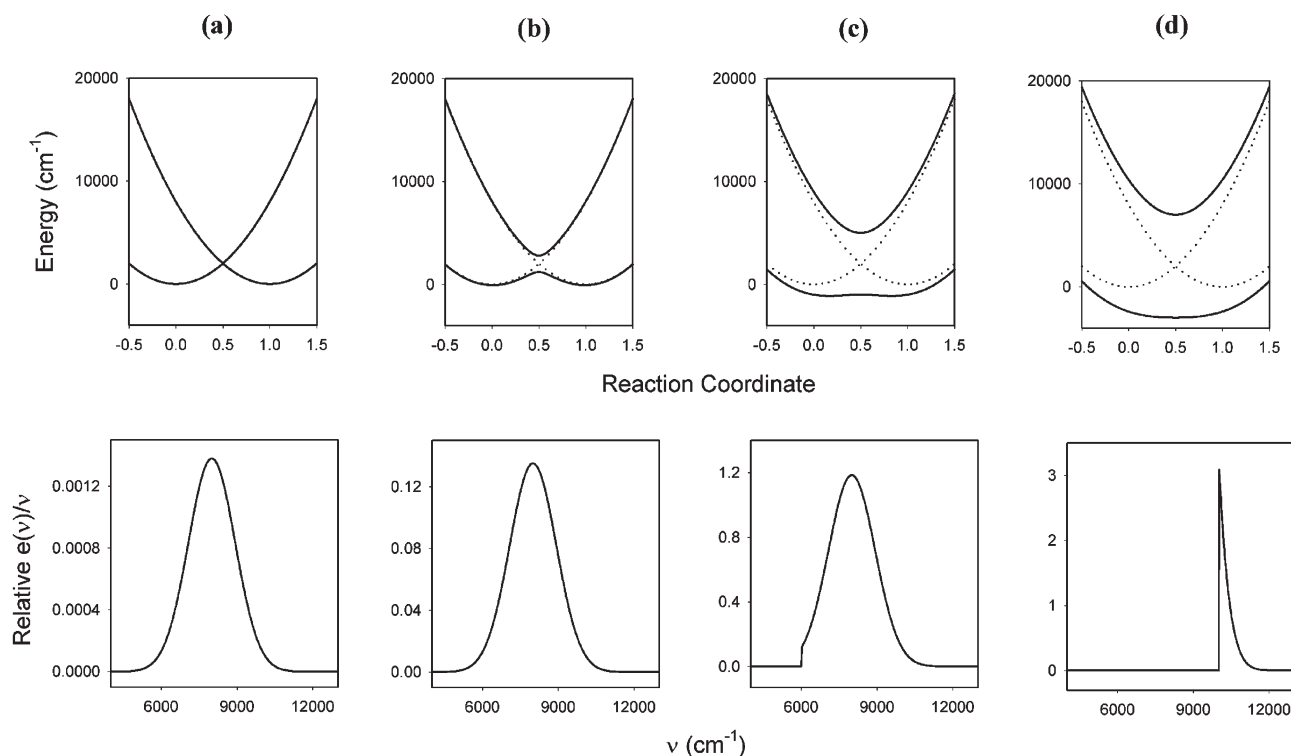
Fig. 2 Potential energy surfaces and band-shape predictions from the two-state classical model. Plots of the energy *versus* reaction coordinate (top panel) and the relative reduced absorption spectra ε/ν *versus* ν (lower panel) for a symmetrical mixed-valence system with increasing $2H_{ab}/\lambda$ ($\lambda = 8000$ cm^{-1}). The values of $2H_{ab}/\lambda$ (H_{ab}, in cm^{-1}) are (a) 0.02 (80), (b) 0.2 (800), (c) 0.75 (3000), and (d) 1.25 (5000) (adapted from ref. 14).

The band cut-off effect is manifested by IVCT bands which are Gaussian on the high energy side and skewed on the low energy side. The physically-unrealistic nature of the sharp spectral cut-off is attributed to the neglect of quantum effects and solvent broadening of the individual vibronic components which "round-off" the abrupt spectral cut-off. As indicated in Fig. 2, the effect does not become significant until H_{ab} exceeds $\lambda/4$, and $\Delta v_{1/2}$ is equivalent to $\Delta v_{1/2}^{\circ}$ for $2H_{ab} < \lambda - [4RT\ln2]^{1/2}$.[14] Beyond this regime, $\Delta v_{1/2}$ decreases relative to $\Delta v_{1/2}^{\circ}$ with increasing H_{ab} and the IVCT bands increase in intensity until $2H_{ab} = \lambda$ at the transition between Class II and Class III. At this point, the band retains intensity in the higher energy half only. The H_{ab} values determined from eqn (9) are increasingly underestimated as the system approaches the borderline between Class II and Class III, and this underestimation reaches 50% when $2H_{ab} = \lambda$.[13] For $2H_{ab} > v_{max}$, only the high energy side remains and the asymmetrically-shaped band shifts to higher energy, increases in intensity, and narrows due to the greater curvature at the E_+ minimum {Fig. 2(d)}.[13,14] An IVCT band which exhibits a cut-off effect should become increasingly symmetrical as the temperature is decreased.[12]

The explicit consideration of this effect is required for the accurate analysis of the IVCT bands of moderately- to strongly-coupled systems. Brunschwig, Creutz and Sutin have proposed relationships between the IVCT energies and bandwidths which enable the calculation of corrected values for H_{ab} through the introduction of an error function.[14] The treatment of symmetrical mixed-valence systems[14] has subsequently been extended to unsymmetrical systems[21] in which the Gaussian-shaped band is centred at $\lambda + \Delta E_0$ and exhibits a cut-off at $2H_{ab}$.

3.3 Classifying mixed-valence systems between the Class II and Class III regimes

The cut-off effect has been observed in the spectra of both organic and transition metal-centred mixed-valence species, and has been utilised as a diagnostic marker for systems which lie close to the transition between the localised (Class II) and delocalised (Class III) regimes.[4,5,12–14] While the majority of reports have considered the relative magnitudes of $2H_{ab}$ and λ as the criterion for defining the position of a mixed-valence system between the two regimes, alternate criteria have been proposed.

Nelsen[13] considered the disappearance of the electron transfer barrier as an indication of the shift from Class II to the borderline between Class II and Class III. By factoring the semi-classical expression for E_{th} in eqn (7), the parameter F was defined as the fraction of the electron transfer barrier remaining after the inclusion of electronic coupling {eqn (16)}. The magnitude of F varies between 1 (in the limit of complete localisation) and 0 (at the borderline between Class II and Class III).

$$E_{th} = F(v_{max}/4) \text{ where } F = (1 - 2H/v_{max})^2 \qquad (16)$$

The magnitudes of F determined on the basis of electronic coupling values from the Hush model[1] (with $H = H_{ab}$) and CNS model[15,18] (with $H = H_{M_1 M_2}$) were compared[13] for the series of 1,4-dicyanamidobenzene complexes[22] including

$[\{Ru(NH_3)_5\}_2(\mu\text{-}BL)]^{3+}$, $trans,trans\text{-}[\{Ru(NH_3)_4(py)\}_2(\mu\text{-}BL)]^{3+}$ and $mer,mer\text{-}[Ru(NH_3)_3(bpy)\}_2(\mu\text{-}BL)]^{3+}$ {where BL represents the dianions dicyd^{2-} (1,4-dicyanamidobenzene), Me$_2$dicyd^{2-} (1,4-dicyanamido-2,5-dimethylbenzene) and Cl$_4$dicyd^{2-} (2,3,5,6-tetrachloro-1,4-dicyanamidobenzene)}. F decreased with progressively stronger electronic coupling as BL was varied through the series Cl$_4$dicyd^{2-}, dicyd^{2-} and Me$_2$dicyd^{2-}. While the values of F_{Hush} and F_{CNS} were comparable in the absence of significant IVCT band cut-off effects, the CNS method provided more reasonable estimates of the degree of coupling near the borderline between Class II and Class III.[13] The H_{ab} values determined from the Hush model {eqn (9)} were increasingly underestimated as the borderline was approached, due to cut-off effects and discrepancies between the effective charge transfer distance and the geometrical metal–metal distance. While the magnitude of F provides a suitable means to assess the relative degree of electronic coupling within a series of closely-related complexes in the localised regime,[13] the criterion is inappropriate for strongly-coupled systems which exhibit highly asymmetric IVCT bands. The latter typically require at least a three-state analysis.

As an alternative classification scheme, Brunschwig, Creutz and Sutin[14] introduced a criterion based upon the experimental and predicted IVCT bandwidths,[1] according to eqn (17). The magnitude of the Γ parameter distinguishes the class of a mixed-valence system: $0 < \Gamma < 0.1$ for weakly-coupled Class II systems, $0.1 < \Gamma < 0.5$ for moderately-coupled Class II systems, $\Gamma \approx 0.5$ at the transition between Class II and Class III, and $\Gamma > 0.5$ for Class III systems.

$$\Gamma = 1 - (\Delta v_{1/2})/(\Delta v_{1/2}^{\circ}) \qquad (17)$$

The classification of a number of mixed-valence systems based on the magnitudes of Γ were shown to be in favourable agreement with the results from prior experimental studies.[14] For $[\{Ru(NH_3)_5\}_2(\mu\text{-}4,4'\text{-}bpy)]^{5+}$ (4,4'-bpy = 4,4'-bipyridine), for example, the Γ value of -0.1 was consistent with a Class II assignment, as established previously from the broad, Gaussian-shaped and solvent-dependent IVCT band.[14] A delocalised assignment was favoured for the Creutz–Taube ion, $[\{Ru(NH_3)_5\}_2(\mu\text{-}pyz)]^{5+}$ (pyz = pyrazine), on the basis of the Γ value of 0.63 for the narrow ($\Delta v_{1/2} = 1480$ cm^{-1}) asymmetrically-shaped IVCT band at 6320 cm^{-1} (in DCl/D$_2$O).[2] This classification was consistent with the findings from an extensive series of physical techniques of varying timescales[4,5,12,23] including IR, single crystal EPR, Stark effect and Raman spectroscopy.[3]

While the Γ bandwidth criterion provides a reasonable qualitative measure for the classification of mixed-valence systems between the localised and delocalised limits, band-shape analyses are frequently complicated by a number of factors. These include multiple overlapping IVCT and IC transitions,[11,12] differences in the extent of electronic delocalisation between the ground and mixed-valence excited states, contributions from vibronic progressions, and multiple nuclear and solvent vibrations which are coupled to the electron transfer.[12]

This journal is © The Royal Society of Chemistry 2006

Chem. Soc. Rev., 2006, **35**, 424–440 | 429

4. Theoretical models for the treatment of systems between the localised and delocalised regimes

4.1 Three- and four-state classical models

Classical models are the preferred method of analysis for IVCT transitions due to the facility of their application and their overlap with the Marcus theory of electron transfer.[1] However, the classical two-state approximation is based upon the Born–Oppenheimer approximation and is strictly valid only in the strongly localised and delocalised limits. In real systems, the inclusion of additional electronic states is often necessary to account for the role of the bridging ligand in mediating the superexchange coupling between the metal-based sites.

The three-state model proposed by Brunschwig, Creutz and Sutin[14] provides an extension to the two-state classical model by explicitly including a third electronic state formed by charge transfer to or from the bridging ligand. The influence of this additional state depends upon its energy {H_c in eqn (18)} relative to the other two diabatic states {H_a and H_b in eqn (2)}. ΔE_{ac} represents the energy difference between the minima of the potential energy surfaces for states 'a' or 'b' and the bridge state 'c'.

$$H_c = \lambda(X - 0.5)^2 + \Delta E_{ac} \qquad (18)$$

The salient features of the three-state model are considered here for a symmetrical mixed-valence system, where the mediating state lies above the intersection of the reactant and product diabatic states at $X = 0.5$.[14] The adiabatic surfaces are obtained solving a 3×3 Hamiltonian analytically or numerically. The electron transfer process involves super-exchange coupling of the three states, where states 'a' and 'b' couple to state 'c' through the electronic coupling parameter H_{ac} (= H_{bc}), and the direct H_{ab} coupling is zero. The diabatic and adiabatic potential energy surfaces, and the corresponding absorption spectra for a series of H_{ac} coupling strengths are illustrated in Fig. 3, where λ and ΔE_{ac} are 8000 and 16 000 cm^{-1}, respectively.

The major difference between the two- and three-state models is the allowance in the latter for a second absorption (generally MLCT) at higher energy than the IVCT. As H_{ac} (= H_{bc}) increases in the Class II regime {Fig. 3(a) and (b)}, the intensity of the IVCT transition increases. The MLCT intensity initially increases before reaching a maximum and decreasing to the borderline between Class II and Class III, at which point the band vanishes {Fig. 3(c)}. While $\nu_{max} = \lambda$ in the Class II regime for the two-state model, in the three-state case ν_{max} is initially equal to λ in the Class II limit, but decreases as the borderline between Class II and Class III is approached. ν_{max} increases as does H_{ac} in the Class III regime for the three-state case {Fig. 3(d)}. The inclusion of a fourth electronic state is required to qualitatively reproduce the experimental observation of MLCT transitions for Class III complexes.[14]
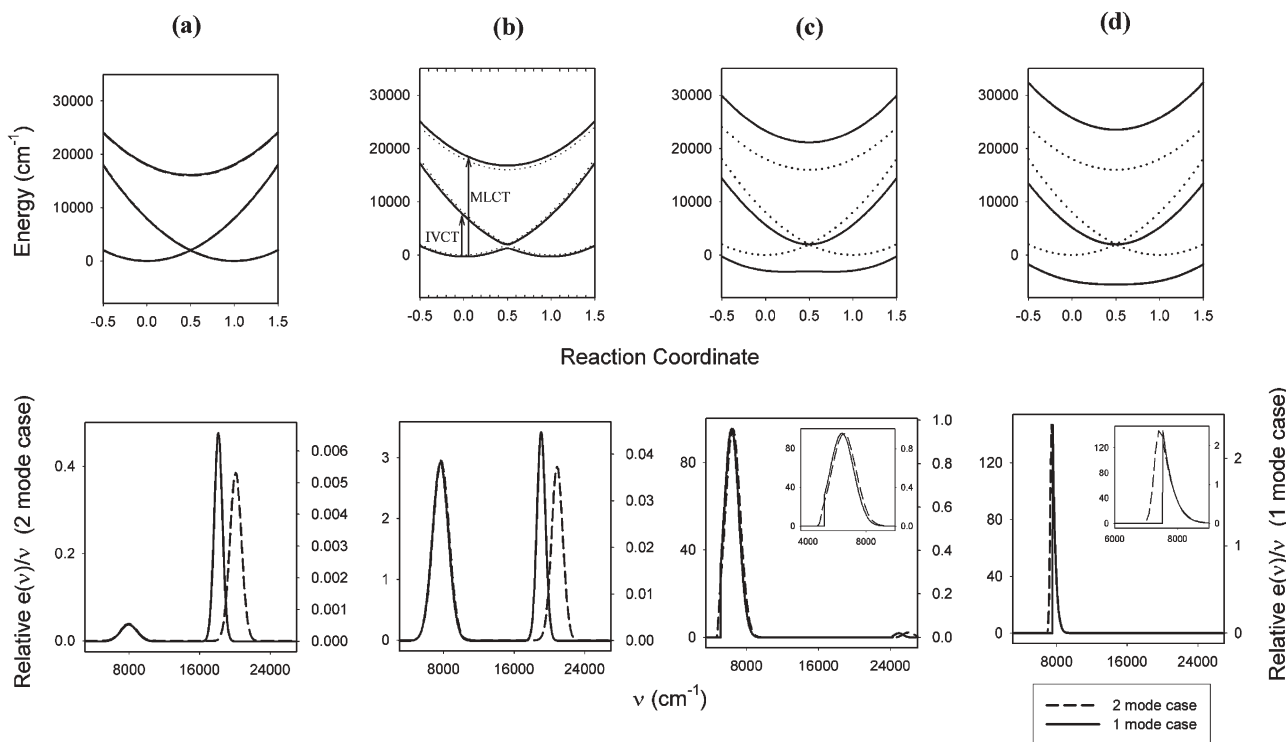
Fig. 3 Potential energy surfaces and band-shape predictions from the three-state classical model.[14] Plots of the energy *versus* reaction coordinate for the three-state one-mode model (top panel) and overlay of the reduced absorption spectra ε/ν *versus* ν (lower panel) for a symmetric mixed-valence system with increasing values of H_{ac} (λ = 8000 cm^{-1}, ΔE_{ac} = 16 000 cm^{-1}) for the one- (- - -) and two-mode (—) cases. The values of H_{ac} in cm^{-1} are (a) 800, (b) 2400, (c) 7000, and (d) 9000. The transition between Class II and Class III occurs at H_{ac} = 8000 cm^{-1}. (The numerical codes used for the construction of the potential energy surfaces and resulting spectra were provided by Dr Gerald Sando[21] and were implemented within Mathcad 2001 Professional using internal algorithms for matrix diagonalisation.)

The symmetric vibration mode. Within a three-state two-mode approach,[14] the addition of a second vibrational mode representing a symmetrical combination of stretches results in a smooth spectral cut-off. Fig. 3 depicts the potential energy surfaces and corresponding absorption spectra. The energies of the diabatic states are expressed in eqn (19) where X_1 and X_2 represent the anti-symmetric and symmetric reaction coordinates, respectively. In the Class II regime, the addition of the symmetric vibration mode has a modest effect only on v_{max} and $\Delta v_{1/2}$ {Fig. 3(a) and (b)}. In Class III, the IVCT band is broadened and the spectral cut-off is smoothed out relative to the one-mode two- and three-state models {Fig. 3(d)}.

$$H_a = \lambda X_1^2 + \lambda X_2^2$$
$$H_b = \lambda (X_1 - 1)^2 + \lambda X_2^2 \qquad (19)$$
$$H_c = \lambda (X_1 - 0.5)^2 + \lambda (X_2 - 0.5)^2 + E_{ac}$$

The central role of the symmetric vibration mode for moderately- to strongly-coupled mixed-valence systems was first discussed by Hush,[23] and arises from the symmetrical nature of the electronic redistribution that occurs on charge excitation. The IVCT transition originates from a state in which the electron is predominantly localised on a metal site, to one on the bridge. The latter is displaced from the metal-localised state along the totally symmetric vibration coordinate, and the vertical IVCT excitation occurs from the ground state surface to a region on the upper surface that is higher up, and therefore steeper. The addition of the symmetric mode results in a broadening in the IVCT and MLCT bands with increasing delocalisation.

4.2 Vibronic coupling models: the PKS model

Quantum mechanical treatments account for the integral role of *vibronic coupling* which becomes increasingly important with stronger electronic coupling due to the dynamic interaction between the vibrational and electronic motions (*i.e.* the failure to meet the Born–Oppenheimer approximation). The PKS model proposed by Piepho, Krausz and Schatz was originally formulated as a two-state, one-dimensional model along an anti-symmetric vibrational coordinate, q.[24a,b] The vibronic energy levels are determined using wavefunctions which allow for the dependence on *both* the nuclear and electronic coordinates, and the IVCT manifold is calculated as a superposition of the transitions between these levels. The model was the first to investigate the full IVCT absorption profile by iteratively fitting the band to three parameters: the electronic and vibronic coupling parameters (ε and λ, respectively) and the wavenumber of the totally symmetric metal–ligand stretching vibration ($\bar{v}$). The energies of the surfaces, $E_{1,2}$(PKS), and the expressions for the PKS parameters are given by eqn (20a) and (20b), where c is the speed of light, f is the metal–ligand force constant and μ is the reduced metal–ligand mass.[4] The localised limit occurs when $\varepsilon \approx 0$ and $E_2 - E_1 \approx 2\lambda q$, and the delocalised limit when $\lambda \approx 0$ and $E_2 - E_1 \approx 2\varepsilon$.

$$E_{1,2}(\text{PKS}) = \frac{q^2}{2} \pm \left(\varepsilon^2 + \lambda^2 q^2\right)^{1/2} \qquad (20a)$$

$$v_{max} = 2\lambda^2 \bar{v}, \; H_{ab} = \varepsilon\bar{v} \text{ and } \bar{v} = 1/c \; (f/4\pi^2\mu) \qquad (20b)$$

The PKS treatment has been successfully applied to simulate the IVCT bands of a range of systems which lie between the fully localised and delocalised regimes.[24] While the method reproduces the salient features of the localised-to-delocalised regime—including the increasing intensity and narrowness of the IVCT bands—Reimers and Hush have argued that the treatment is flawed in several fundamental aspects of its design and application.[23] Most importantly, the model neglects the central role of the bridging ligand in mediating the charge transfer transition between the metal centres. In response to these criticisms, the PKS model has been extended to include coupling to multi-centre vibrations, solvent and symmetric vibration modes.[24c]

4.3 Molecular orbital models: the Ondrechen model

The three-state molecular orbital model proposed by Ondrechen and coworkers[25a–c] for delocalised mixed-valence systems was the first to accommodate the effects of excitations in the totally symmetric vibration modes. The two metal-based states of the dinuclear complex are each coupled to one local vibrational degree of freedom, and interact *indirectly via* a third electronic state localised on the bridging ligand. Each terminal state is separated from the bridging ligand state by an energy gap α, which is typically estimated from the difference in potentials between the metal-based oxidation and ligand-based reduction potentials. The coupling between the states is represented by the electron-exchange coupling constant, J, which quantifies the donor-bridge and acceptor-bridge interactions, rather than the *direct* donor–acceptor interaction. The three-state delocalised system is constructed from symmetric and anti-symmetric combinations of the initial unperturbed electronic states, as depicted schematically in Fig. 4. The IVCT transition arises from electron transfer between the bonding (B) and non-bonding (N) orbitals within the molecular orbital manifold of the mixed-valence system. Like the PKS model, the Ondrechen model involves parameter fitting through the simulation of the absorption spectrum for the mixed-valence species.
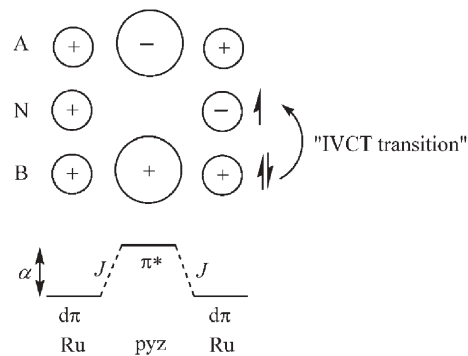
Fig. 4 Qualitative molecular orbital diagram for a mixed-valence complex such as $[\{Ru(bpy)_2\}_2(\mu\text{-pyz})]^{5+}$ according to the three-state model. The bonding, B (symmetric), non-bonding, N (node on the bridging ligand) and antibonding, A (anti-symmetric) molecular orbitals are shown. The "IVCT transition" corresponds to a bonding → non-bonding transition with energy $E_{B \rightarrow N}$.

This journal is © The Royal Society of Chemistry 2006

Chem. Soc. Rev., 2006, **35**, 424–440 | 431

The energy of the IVCT transition ($E_{B \to N}$) is given by eqn (21). In the limit of large exchange coupling, the magnitude of $E_{B \to N}$ is dominated by the value of J and modified only slightly by α. This represents a key difference between the Ondrechen model and the two-state semi-classical model in which the energy of the IVCT band is λ {eqn (5)}. In the former, eqn (21) accounts for the appearance of high energy IVCT bands for delocalised complexes with minimal reorganisational energies.

$$E_{B \to N} = -\frac{1}{2}\left(\alpha - \sqrt{\alpha^2 8 J^2}\right) \qquad (21)$$

The Ondrechen model has been applied to simulate the IVCT line-shape for the Creutz–Taube ion, in which the two Ru(dπ) and vacant pyz(π*) orbitals form bonding (fully-occupied), non-bonding (half-occupied) and antibonding (unoccupied) combinations of molecular orbitals (Fig. 4).[25a,b,25d] The IVCT band at 6320 cm^{-1} was assigned as a B $\to$ N transition. Importantly, this transition exhibits a *dual* nature: it contains IVCT character due to the transition from a sum to a difference combination of Ru(dπ) orbitals, in addition to LMCT character due to the redistribution of charge from the node on pyz in the non-bonding state to the two metal centres.[25d] The latter is accompanied by a change in the metal–ligand bond lengths on *both* sides of the bridge. The symmetric vibrations coupled to the two sites and the symmetric modes of the bridging ligand itself are vibrationally coupled to the electronic transition.[23] Qualitatively, this coupling is manifested by a small blue-shift and increased line-width in the absorption band.[25a] Resonance Raman experiments on delocalised mixed-valence systems with excitation in the B $\to$ N transition reveal significant resonant enhancement of symmetric bridging ligand modes. Such enhancements have been observed for both the Creutz–Taube ion[2] and for the pyz-bridged "dimers-of-trimers", [{Ru$_3$(μ_3-O)(μ-O$_2$CCH$_3$)$_6$(CO)(L)}$_2$(μ-pyz)]$^-$ {L = 4-(dimethylamino)pyridine, pyridine, 3- or 4-cyanopyridine}.[26] The results indicated that ground state delocalisation in these systems could be described by a three-site, rather than two-site mixing mechanism. The Ondrechen model has been extended to include vibronic coupling, and to a five-state treatment with two coupled vibrations.[25d,26] However, the model has been criticised due to complications with the treatment of near-degenerate orbitals and spin–orbit coupling effects.[25c,26]

4.4 Computational approaches and quantum mechanical methods

Semiempirical computational methods such as INDO, AM1 and PM3, and *ab initio* methods such as Density Functional Theory (DFT) have been extensively employed to provide rapid calculations of the structural and electronic properties of mixed-valence systems.[2,27,28a,b] The electronic structures of the systems are generally treated by a two-state model in which the donor–acceptor interaction is quantified by an electronic coupling parameter, and the environment surrounding the system is treated as a dielectric continuum.

Reimers, Hush and coworkers have recently proposed an extensive theoretical and computational framework for quantitatively modelling the electronic characteristics of mixed-valence systems between the localised and delocalised regimes.[23] The formalism accounts for the key features of the shift, including the central role of both anti-symmetric and symmetric modes within the full treatment of the vibronic coupling problem. The application of these formalisms has been facilitated by the development of fast numerical methods using high level *a priori* computational calculations such as DFT and *ab initio* techniques.[23] The success of the methodology has recently been demonstrated by providing a unified description to correlate the molecular structure and photosynthetic function of the special pair in bacterial photosynthesis using a four-state seventy-mode model.[29] The model has also been applied to mixed-valence systems such as the Creutz–Taube ion,[23] and has enabled the elucidation of several key features regarding the interplay of symmetric and anti-symmetric modes. Importantly, in the weak-coupling limit, displacements in the anti-symmetric modes control the energy levels and the presence of vibronic coupling through the symmetric modes is of minor importance. By comparison, in the strong coupling limit, displacements in the symmetric modes dictate the energy levels, and vibronic coupling through the anti-symmetric modes is relatively less important.[23]

4.5 Towards a "unifying theory" for IVCT

The above-mentioned models (§4.1–4.4) capture the essence of the shift between the localised and delocalised regimes, and demonstrate that a unifying theory must embody all of the features; *i.e.* the explicit inclusion of the bridging ligand and anti-symmetric and symmetric modes within the full treatment of a vibronic coupling problem.[12,23] Importantly, such a theory must be parameterised in terms of physically transparent quantities which are amenable to experimental analysis.[8,11,12] A key realisation is that nuclear dynamics are important even for formally delocalised complexes which can display a large range of behaviours depending on their degree of delocalisation.[12] In reality, the transition between localisation and delocalisation is not abrupt, and the explicit distinction between the two regimes is a semantic rather than physical one.

5. The fundamental factors governing the evolution from localised to delocalised behaviour

5.1 Dynamic considerations and the Class II–III classification

The elucidation of the factors which govern the shift between localisation and delocalisation is complicated by the interplay between the timescales for intramolecular electron transfer and the coupled nuclear and solvent vibrations. A recent seminal review by Meyer and coworkers[12] addressed these issues, by defining mixed-valence systems in the "localised-to-delocalised" regime as Class II–III.

Within the semi-classical formalism, the lower frequency solvent modes are treated classically, while the collective higher frequency inner-shell vibrations are treated quantum mechanically (*i.e.* $\lambda = \lambda_o + \Sigma\lambda_i$).[12] As H_{ab} increases in a closely-related series of complexes, the barrier to electron transfer decreases, as does the timescale for this process. If the solvent barrier is initially eliminated ($\lambda_o < \Sigma\lambda_i$), then the solvent modes for the donor and acceptor sites are averaged in the region where

$\lambda_o < 2H_{ab} < \lambda_o + \Sigma\lambda_i$. However, the two sites remain structurally distinct and will exhibit localised oxidation states. This scenario occurs if the rate of electron transfer, k_{et}, is intermediate between the frequencies for solvent reorientations $(10^{11}–10^{12} \text{ s}^{-1})$ and bond vibrations $(10^{13}–10^{14} \text{ s}^{-1})$, such that $k_{et} \sim 10^{12}–10^{13} \text{ s}^{-1}$ and $0.7 < 2H_{ab}/\lambda < 1$. On this basis, operational definitions for the various classes have been proposed: in Class II the solvent and exchanging electron are localised; in Class II–III the solvent modes are averaged but the exchanging electron is localised; and in Class III, the exchanging electron is delocalised and the solvent and vibrational modes are averaged. Although a system is considered to be fully delocalised when $2H_{ab} > \lambda$, the effects of transient charge localisation may still be observed on the IR timescale for a borderline Class III system.[12,14]

The classification of mixed-valence systems is not straightforward and relies on observations from several experimental techniques with widely different timescales.[12] The appearance of IVCT bands and their solvent dependence provides the most useful experimental criterion for distinguishing between Classes II (broad, solvent-dependent, localised oxidation states) and II–III (narrow, solvent-independent, localised oxidation states). The appearance of symmetrical bridging ligand stretch vibrations {such as $v(\text{pyz})$, $v(N_2)$ or $v(CO)$} on the $\leqslant 10^{-11}$ s IR timescale provides one of the most reliable markers for electronic localisation.

5.2 Probing the factors which govern the shift between the localised and delocalised regimes

Experimentally, the factors which govern the shift between the localised and delocalised regimes have been probed by the dependence of the IVCT characteristics on structural and substitutional changes in mixed-valence complexes, such as the distance between the metal centres,[1] the ability of the bridging ligand to delocalise the electronic charge,[13] as well as the identity and coordination environments of the metal centres.[4–7,9,10,12] Variations in the external environment such as the identity and composition of the solvent, the temperature, and anions in the surrounding medium also provide critical contributions to the electron transfer barrier.[11]

5.2.1 The role of the bridging ligand: structural and electronic considerations. Bridging ligands provide the linkage of metal centres in polynuclear complexes and control the distance and relative orientation of the components, as well as the inter-component electron and energy transfer processes. The role of the bridging ligand has been extensively documented and reviewed[6,7,19,20,27,30] and the pertinent theoretical issues only are mentioned here.

For a dinuclear ligand-bridged complex, the coupling between the donor and acceptor can occur directly *via* a through-bond mechanism, or indirectly *via* a through-space superexchange process where the bridging ligand mediates the donor–acceptor coupling. In reality, the operative mechanism of delocalisation can involve both contributions. Superexchange theory provides a conceptual framework for bridging ligand effects in intramolecular electron transfer.[19,20] Electronic coupling between the two metal-based units may
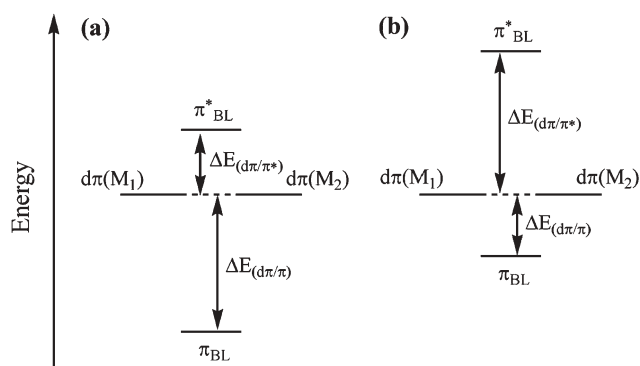
Fig. 5 Schematic energy level diagrams for superexchange-assisted electronic coupling *via* (a) an electron transfer mechanism or (b) a hole transfer mechanism. M_1 and M_2 denote the metal centres and BL denotes the bridging ligand.

comprise bridge-mediated electron transfer (which utilises the lowest unoccupied molecular orbitals, LUMOs, of the bridge) or hole transfer (which utilises the highest occupied molecular orbitals, HOMOs, of the bridge) as shown in Fig. 5. The parameters which are effective to describe the through-bond interaction are the overlap between the frontier orbitals of the metals {$d\pi(M_1)$ and $d\pi(M_2)$} and the bridging ligand (π_{BL} and π_{BL}^*), and the electronic interactions between the atoms of the bridge connecting the frontier units to one another.

Class I or weakly-interacting Class II polymetallic complexes comprising two or more non-interacting sites will exhibit a superposition of the individual properties of the constituent sub-units and are known as supramolecular assemblies.[30] Interacting sites permit the possibility of long-range and vectorial energy or electron transfer processes and are generally Class II or III systems.

5.2.2 The effective electron transfer distance: Stark effect spectroscopy. While, the geometrical metal–metal separation (r_{geom}) is often employed instead of r_{ab} to calculate H_{ab} from eqn (9) and (10), the values determined in this way are lower limits only for the electronic coupling.[12] Electroabsorption (Stark effect) spectroscopy on the IVCT bands of dinuclear mixed-valence complexes provides a powerful technique to determine the *effective* electron transfer distances (r_{12}) from the change in dipole moment for the IVCT transition, $|\Delta\mu_{12}|$, according to eqn (22). r_{ab} is subsequently determined from eqn (23).

$$r_{12} = |\Delta\mu_{12}|/e \qquad (22)$$

$$r_{ab} = [(r_{12})^2 + (|\mu_{12}|)^2]^{1/2} \qquad (23)$$

The Stark absorption experiment measures the change in the absorption spectrum, $\Delta A(v)$, for an isotropic and immobilised sample in response to an applied electric field, F_{ext} (typically 1–4 MVcm^{-1}), and has been the subject of a number of comprehensive reviews.[5,31] The analysis is typically performed according to the classical treatment of Liptay, in which the $\Delta A(v)$ *versus* v spectrum is fitted by a linear combination of the zeroth-, first- and second-derivatives of the unperturbed

This journal is © The Royal Society of Chemistry 2006

Chem. Soc. Rev., 2006, **35**, 424–440 | 433

absorption spectrum.[32] The contributions of the derivative components provide information on changes in the transition dipole moment, the excited state/ground state polarisability and dipole moment differences, respectively. Stark effect spectroscopy thus permits an independent determination of H_{ab} *via* eqn (10) by providing an accurate measure of r_{ab}.[14,33] The adiabatic description reveals partial delocalisation as a reduction in r_{12} (the *effective* charge transfer distance) relative to r_{ab} (the true distance), while the diabatic description reveals delocalisation as a reduction in the amount of charge (Δq) actually transferred.

Stark effect measurements for dinuclear mixed-valence ruthenium and osmium complexes frequently yield effective charge transfer distances which are a fraction only of the geometrical inter-metal distances.[31] For example, the IVCT band at 6320 cm^{-1} in the Creutz–Taube ion yielded a dipole moment change of 0.7 ± 0.1 D, compared with the value of 32.7 D expected for unit charge transfer across the full geometrical distance.[31a] It must be noted that while the Liptay analysis is applicable to complexes in the weak-coupling Class II and fully-delocalised Class III regimes, this classical approach is inappropriate for systems in the intermediate localised-to-delocalised regime.

5.2.3 Solvent reorganisational contributions. The sensitivity of the IVCT transition to solvent variation is generally accepted as a criterion for distinguishing between localisation or delocalisation.[4–8,11,12] The latter is exemplified by the negligible solvent dependence of the IVCT band for $[\{Ru(bpy)_2\}_2(\mu\text{-pyz})]^{5+}$, in contrast to the solvent-dependent band for the localised system $[\{Ru(bpy)_2\}_2(\mu\text{-}4,4'\text{-bpy})]^{5+}$.[2]

While the predictions of the dielectric continuum model {eqn (11)} have been verified in a number of IVCT solvatochromism studies of mixed-valence ruthenium complexes,[11] the model breaks down when the underlying assumptions of the classical treatment are invalidated, or in the presence of specific solvent–solute interactions and ion-pairing contributions. As an alternative to the spherical cavity approximation, ellipsoidal cavity models have been developed within the classical formalism to provide a more physically realistic description for the non-spherical structures of dinuclear complexes.[11]

Experimentally, the analysis of IVCT solvatochromism data according to dielectric continuum models has often been severely complicated by non-continuum effects, which has motivated extensive experimental, theoretical and computational studies on the microscopic basis of solvent reorganisation.[8,11] The experimental strategy for extracting information at the molecular level using IVCT solvatochromism studies involves probing the first solvation shell separately from the bulk solution. Dinuclear ruthenium complexes incorporating ammine and cyano ligands have been extensively investigated in this regard, due to the existence of strong directional H-bonding and donor–acceptor interactions between the chromophore ligands and individual solvent molecules.[11] Correlations have been found between the IVCT solvent shifts and empirical solvent parameters such as the Gutmann donor and acceptor numbers (denoted by DN and AN, respectively). In studies of dinuclear ruthenium mixed-valence complexes

based on $Ru(NH_3)_5$, *trans*-$Ru(NH_3)_4(py)$ and $Ru(bpy)(NH_3)_3$ with pyz, 4-cyanopyridine and 4,4'-bpy bridging ligands,[11] the IVCT energies correlated linearly with DN, and the magnitude of the specific interaction increased with the donor number of the solvent, and the number of NH_3 ligands in the chromophore. The specific solvation effects occur preferentially at the Ru^{III} coordination sphere of the mixed-valence $[Ru^{II}Ru^{III}]$ chromophore, and introduce an additional solvent trapping barrier which represents a redox asymmetry contribution (ΔE_0).

In parallel with experimental investigations, considerable attention has been directed to the development of computational methods which are parameterised in terms of continuum and non-continuum solvation effects in order to provide a physically realistic treatment of solvation under experimental conditions.[8,11] While semi-empirical methods often fail to provide an adequate representation of intermolecular interactions due to their treatment of the solvent as a dielectric continuum, the ZHR-SS method developed by Zeng, Reimers and Hush is parameterised in terms of explicit solvent dipoles for the first solvation shell, while the bulk solvent is treated as a dielectric continuum.[28a,b] The equilibrium ground-state solvent structure is determined by standard Monte Carlo or molecular dynamics simulations, and *ab initio* methods are employed to calculate the energy, charge distribution and polarisability of the solute from sampled configurations. The strength of the ZHR-SS method lies in the explicit solvent structure approach, albeit at the cost of a full liquid structure simulation.

The development of practical computational procedures to model and predict intramolecular electron transfer properties, using input from electronic structure calculation methods for the complexes and molecular theories of solvation, have been impeded by limited experimental data.[8,11,28a,b] There is clearly a need for experimental studies of IVCT solvatochromism which provide insights into microscopic solvent reorganisational contributions.

5.2.4 Structural and environmental contributions to the redox asymmetry. Redox asymmetry (ΔE_0) contributions are typically assessed experimentally within the classical framework, and provide a means of inducing localisation in a valence-delocalised complex. Central to the two-state classical analysis is the assumption that a ΔE_0 contribution is manifested spectroscopically as an equivalent variation in v_{max} {according to eqn (1)} at constant H_{ab} and λ. Redox asymmetry effects have been probed through direct perturbation of the inner coordination sphere by terminal ligand substitution, conformational variations in the bridging ligand structures, the incorporation of unsymmetrical bridging ligands, or the use of hetero-dinuclear complexes.[4,7,11] Environmental ΔE_0 contributions include ion-pairing, encapsulation, pH and temperature effects, in addition to specific solvation effects involving H-bonding interactions with the bridging or terminal ligands.

Curtis and coworkers[34a,b] have proposed a semi-quantitative interpretation for ΔE_0 effects, based on a classical two-state perturbation treatment and electrochemical potential measurements. According to eqn (24), a quantity m' is defined as the ratio of the shift in the electrochemical potential at the

indirectly perturbed redox site 'a' {$\delta E_{ox}(Ru_b)$} to the shift at the *directly* perturbed redox site 'b' {$\delta E_{ox}(Ru_a)$}, and a quantity ρ is defined as the ratio of the coefficients for the diabatic wavefunctions (Ψ_a and Ψ_b). The electrochemical shifts are assessed relative to the redox potentials in the unperturbed complex.

$$\rho = (m')^{1/2} = \frac{b}{a} = \left(\frac{\delta E_{ox}(Ru_b)}{\delta E_{ox}(Ru_a)}\right)^{1/2} \quad (24)$$

The parameters a^2 and b^2 represent the fractional valences on the *directly* and *indirectly* perturbed metal centres, respectively {b^2 is equivalent to the delocalisation parameter (α^2) defined by Hush[1]}. Assuming that the overlap between the diabatic wavefunctions is negligible, a^2 and b^2 are obtained from the normalisation condition $a^2 + b^2 = 1$. The parameter ρ is determined from the slope (m) of a plot of the change in the formal potentials of the acceptor *versus* the donor and provides an alternate measure of the extent of electronic coupling between the metal centres, where $0 \leqslant \rho \leqslant 1$, and 0 and 1 are the limits of complete localisation and delocalisation, respectively. Application of the electrochemical analysis to the series of mixed-valence complexes *trans*-[{Ru(NH$_3$)$_5$}(μ-pyz){Ru(NH$_3$)$_4$(L)}]$^{5+}$ {L = NH$_3$, py, 3,5-Me$_2$py, 3-Cl-py, 2,6-Me$_2$pyz},[34c] yielded a value of $\rho = 0.74$ for the Creutz–Taube ion (L = NH$_3$), consistent with a delocalised classification.

Similar yet more subtle ΔE_0 contributions may arise from environmental perturbations such as encapsulation effects.[34d] The addition of the crown ether dibenzo-36-crown-12 to [{Ru(NH$_3$)$_5$}$_2$(μ-pyz)]$^{5+}$ leads to dramatic changes in the IVCT band due to H-bonding interactions between the ammine ligands and the crown ether oxygen atoms. The introduction of the ΔE_0 component on formation of the unsymmetrical 1 : 1 adduct results in a broader and blue-shifted IVCT band as the degree of localisation increases in the nominally valence-delocalised complex. Further addition of the crown ether forms the symmetrical 2 : 1 adduct, and the original line-shape which is indicative of delocalisation is largely restored.

While the majority of IVCT measurements have been performed at high electrolyte concentrations of the tetra-*n*-butylammonium salts of PF$_6^-$, ClO$_4^-$ and halide anions (Cl$^-$, Br$^-$, I$^-$), the analyses have often been conducted without regard for potentially significant ion-pairing and ionic strength effects.[7,11] The IVCT bands for the I$_3^-$ salt of the biferrocenium cation, and the PF$_6^-$ salt of the biferrocenylacetylene cation were blue-shifted with an increase in the ionic strength of the medium, due to ion-pairing between the complex cations and the counter and electrolyte anions.[7,11] Similar effects have been observed for dinuclear ruthenium and iron systems. In all cases, the effects were rationalised on the basis of preferential ion-pairing interactions at the smaller more highly charged M^{III} terminus of [M^{II}M^{III}], resulting in electrostatic stabilisation of the ground state and the introduction of a ΔE_0 component. The ion-pairing contribution has also been assigned as a reorganisational energy due to translation of the counter-ion between the donor and acceptor.[11]

There is currently significant interest in elucidating the microscopic origins of redox asymmetry effects for the extension of vibronic coupling models,[11,23] and the potential application of such effects in molecular switching devices.[7] Recently, the elucidation of ΔE_0 contributions to the IVCT properties of mutants of the photosynthetic reaction centre in purple bacteria has allowed insights into the relationship between structurally-induced perturbations and the mechanism of the photosynthetic function.[23,29] Reimers and Hush[23] have postulated a theoretical treatment to model to the series of unsymmetrical analogues of the Creutz–Taube ion, *trans*-[{Ru(NH$_3$)$_5$}(μ-pyz){Ru(NH$_3$)$_4$(L)}]$^{5+}$ shown in Fig. 6(a). The onset of localisation was accompanied by a significant decrease in H_{ab}, and an increase in λ. Since both quantities should remain constant for a given series of complexes within the classical theory, the results demonstrated that the theoretical treatment of the localised and delocalised transition requires a model in which H_{ab} and λ are allowed to vary with ΔE_0.

5.2.5 Spin–orbit coupling contributions. A complication that must be acknowledged in the analysis of IVCT bands is the existence of multiple underlying IVCT transitions.[12] These arise from the effects of ligand field asymmetry and spin–orbit coupling at low-spin M^{III}(dπ^5) centres (M = Fe, Ru, Os), where the t$_{2g}$ orbitals are split into three dπ levels (Kramer's doublets) which are linear combinations of the d$_{xy}$, d$_{xz}$ and d$_{yz}$ atomic orbitals.[12] As shown in Fig. 6(a), the configurations of the three orbitally non-degenerate states are dπ_1^2dπ_2^2dπ_3^1, dπ_1^2dπ_2^1dπ_3^2 and dπ_1^1dπ_2^2dπ_3^2, in order of increasing energy. The compositions and energy splittings between the levels are
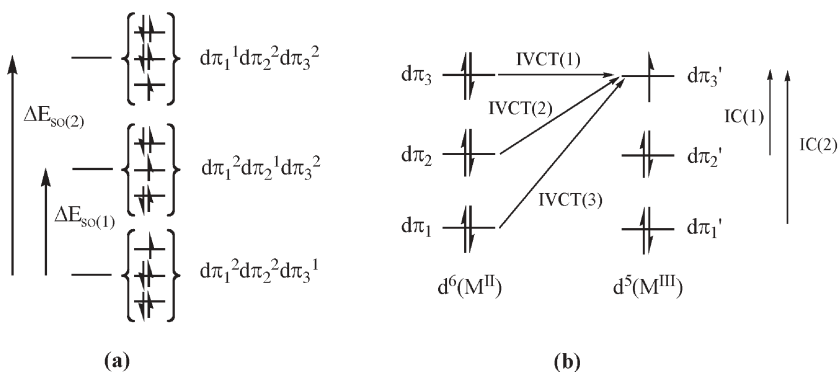
Fig. 6 Schematic illustrations of (a) the IC transitions between the energy levels at an M^{III} centre; and (b) the IVCT and IC transitions in a mixed-valence dinuclear complex, [M^{II}M^{III}].

This journal is © The Royal Society of Chemistry 2006

Chem. Soc. Rev., 2006, **35**, 424–440 | 435

governed by the magnitude of the spin–orbit coupling constant of the metal and the electronic character of the surrounding ligands. Two $d\pi \rightarrow d\pi$ IC transitions between the Kramer's doublets arise due to the formation of the excited states $d\pi_1^2 d\pi_2^1 d\pi_3^2$ or $d\pi_1^1 d\pi_2^2 d\pi_3^2$. These transitions are nominally parity or LaPorte forbidden and are typically observed in the near-IR region as narrow ($\Delta\nu_{1/2} < 1000$ cm^{-1}) solvent-independent bands, e.g. for $[Os^{III}(bpy)_3]^{3+}$ the IC bands occur at 4580 cm^{-1} ($\varepsilon = 450$ M^{-1} cm^{-1}) and 5090 cm^{-1} ($\varepsilon = 360$ M^{-1} cm^{-1}) in CD$_3$CN.[12] In dinuclear mixed-valence systems such as cis,cis-$[\{Os(bpy)_2(Cl)\}_2(\mu\text{-pyz})]^{3+}$, electronic delocalisation across the bridging ligand mixes charge-transfer character into the $d\pi \rightarrow d\pi$ transitions. The IC bands are typically red-shifted and exhibit significantly enhanced intensities compared with their mononuclear analogues.

In addition to two IC transitions, three IVCT transitions arise due to excitation from each of the $M^{II}(d\pi)$ orbitals to the hole at M^{III}, as shown in Fig. 6(b). If the spacing between the spin–orbit states is sufficiently large, three distinguishable IVCT transitions will be observed in the spectra of dinuclear mixed-valence complexes. The larger magnitude of the spin–orbit coupling for Os^{III} relative to Ru^{III} and Fe^{III} $\{\xi \sim 3000 \ (Os^{III}), 1000 \ (Ru^{III}), 800 \ cm^{-1} \ (Fe^{III})\}$[12] typically leads to the observation of a five-band pattern in the IR and near-IR regions, as described in §5.3. The appearance of two discernable IC transitions provides a marker for localisation and a Class II or Class II–III classification.[12] Discrete IVCT components have been observed in a limited number of cases for dinuclear mixed-valence complexes of Ru and Fe, as the lesser $d\pi$–$d\pi$ energy gaps typically result in a broad manifold of three closely-spaced IVCT transitions. The IC transitions are weak, and occur at significantly lower energies compared with their Os analogues. Meyer and coworkers have proposed semi-quantitative relationships between the energies of the IC and IVCT bands in weakly-coupled Class II systems.[12] The energy splittings $\Delta E_{so(1)}$ and $\Delta E_{so(2)}$ {eqn (25)} represent the $\Delta E'$ contribution to the intramolecular electron transfer barrier in eqn (1).

$$\Delta E_{so(1)} \approx \nu_{max}\{IVCT(2)\} - \nu_{max}\{IVCT(1)\} \Delta E_{so(2)} \approx \nu_{max}\{IVCT(3)\} - \nu_{max}\{IVCT(1)\} \quad (25)$$

The recognition of the existence of IVCT spectral components and knowledge of their relative intensities is crucial for the accurate analysis of IVCT bands. The parameters λ_i, λ_o and H_{ab} may differ for the three transitions, and only the lowest energy transition, IVCT(1), corresponds to the thermal electron transfer pathway and can be used to assess the extent of delocalisation in the ground state. The separation between the IVCT components in mixed-valence Ru systems may be estimated from the splitting between the IC bands in their dinuclear Os analogues.[12]

5.3 Experimental studies of mixed-valence systems in the Class II–III regime

Clear examples of localised and delocalised dinuclear systems have been reported in several comprehensive surveys of mixed-valence complexes.[1,4–11] Class II behaviour has been observed in species of the type $[Ru(NH_3)_5\}_2(\mu\text{-BL})]^{5+}$ containing the series of 4,4′-bipyridyl-type bridging ligands shown in Fig. 7(a), and in $[\{Ru(bpy)_2(Cl)\}_2(\mu\text{-pyz})]^{5+}$.[4–7,12] These systems are characterised by broad Gaussian-shaped and solvent-dependent IVCT bands in the near-IR region, which are indicative of weakly-coupled Ru^{II} and Ru^{III} centres.

Dinolfo and coworkers[35] have recently reported rare examples of ligand-based mixed-valency in a series of singly-reduced molecular rectangles, $[\{Re(CO)_3\}_2X]_2\text{-}\mu,\mu'\text{-}(LL)_2$ shown in Fig. 7(b), where X is one of two bridging units (alkoxides, thiazolates or 2,2′-bisbenzimidazolates) and LL is one of a pair of cofacially-aligned redox active ligands. The
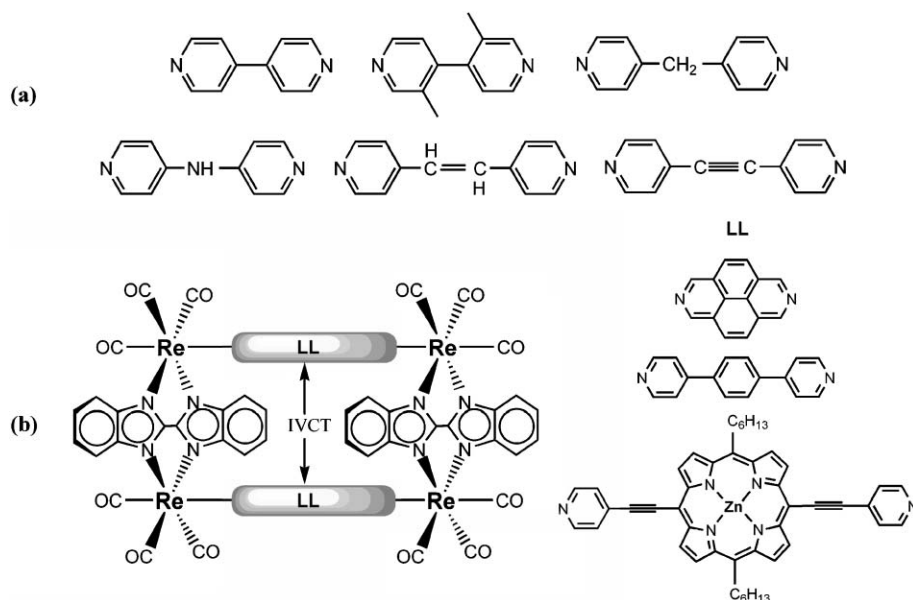
Fig. 7 (a) Examples of 4,4′-bipyridyl-type bridging ligands used in the construction of Class II mixed-valence systems. (b) Molecular rectangles of the form $[\{Re(CO)_3\}_2BiBzIm]_2\text{-}\mu,\mu'\text{-}(LL)_2$, where BiBzIm is 2,2′-bisbenzimidazolate and LL are the cofacially-aligned ligands.[35]

IVCT transitions in the singly-reduced forms originate from direct donor-orbital overlap between the LL moieties, rather than superexchange coupling. The electronic interaction is facilitated by a decrease in the LL/LL approach distance, and an increase in the extent of van der Waals contact and the degree of lateral alignment of LL/LL.[35] These two-state mixed-valence systems lack the complexities in metal-based complexes which occur due to spin–orbit coupling and overlapping IVCT components.

In the Class III systems [{Os(NH$_3$)$_5$}$_2$(μ-BL)]$^{5+}$ {BL = N$_2$, pyz}, the enhanced back-bonding ability of Os relative to Ru leads to electronic delocalisation and averaged valences of +II½.[12] Symmetrical bridging ligand vibrations {v(N$_2$) or v(pyz)} are of low intensity or absent in the IR region, and the spectra *do not* display the expected IC marker bands for Os^{III} which would signal localised oxidation states.

By comparison with these well-defined examples of Class II and Class III behaviour, the classification of the Creutz–Taube ion has been the subject of much controversy.[2] The complex exhibits a narrow ($\Delta v_{1/2}$ = 1480 cm^{-1}), asymmetrically-shaped IVCT band at 6320 cm^{-1} which is comprised of two underlying components centred at 6320 and 7360 cm^{-1}. Relatively weaker narrow bands also appear at 2000, 3200 and 4700 cm^{-1}.[2] The results from an extensive series of experiments including IR, single crystal EPR and Stark spectroscopy led to a consensus in favour of a delocalised ground state for the complex. Resonance Raman measurements revealed a three-state delocalisation mechanism on the basis of the strong coupling of the IVCT transition to a symmetric vibration mode of pyz. A three-state vibronic coupling model, which explicitly includes an electronic state localised on the bridging ligand, is required to fully explain the spectral properties of the ion.[2]

Meyer and coworkers[12] have suggested that the spectroscopic properties of the Creutz–Taube ion may also be consistent with a Class II–III classification. On the basis of a valence-localised ground-state and an electronically delocalised excited state, spin–orbit coupling and ligand-field asymmetry should give rise to three IVCT bands. The two lowest energy transitions were assigned as IC transitions, while the bands at 4700, 6320 and 7360 cm^{-1} were identified as three IVCT transitions {IVCT(1), (2) and (3), in order of increasing energy}. The H_{ab} value of 300 cm^{-1} for IVCT(1) was indicative of a small degree of residual localisation in the ground state, while the mixed-valence excited states {IVCT(2) and (3)} were relatively more delocalised.

Several recent reviews[12–14] have highlighted a number of systems which exhibit Class II–III behaviour. In the mixed-valence complex [{Os(bpy)$_2$(Cl)}(μ-pyz){Ru(NH$_3$)$_5$}]$^{4+}$, there is significant electronic coupling, but also evidence of localised oxidation states in the Os^{III}–Ru^{II} isomer from the appearance of near-IR and IR spectral markers for Os^{III}.[12] Despite the strong electronic coupling between the dπ obitals along the pyrazine axis, a residual barrier to electron transfer exists because the transferring electron at Ru^{II} occupies an orbital which is orthogonal, and only weakly-coupled, to Os^{III}.

Meyer and coworkers have reported an extensive series of Class II–III dinuclear osmium complexes. The symmetrical N$_2$-bridged[12] systems incorporating *cis,cis*-Os(bpy)$_2$(Cl), *trans,trans*-Os(bpy)$_2$(Cl), Os(tpm)(Cl)$_2$ and Os(Tp)(Cl)$_2$ terminal units {tpm = tris(1-pyrazoyl)methane, Tp = tris(1-pyrazoyl)borate} exhibit intense v(N$_2$) stretching vibrations in the IR region which are consistent with electronic localisation on the IR timescale. Each complex displayed five absorption bands in the region 2500–8500 cm^{-1}. The two lowest energy bands were assigned as dπ → dπ transitions at Os^{III} and provided additional evidence for localised oxidation states. The three IVCT transitions at higher energy were narrow and solvent-independent. The related pyz-bridged mixed-valence system, *cis,cis*-[{Os(bpy)$_2$(Cl)}$_2$(μ-pyz)]$^{3+}$, was also assigned to Class II–III on the basis of the characteristic five-band pattern, and the appearance of an intense v(pyz) vibration.[12] *Non-averaged* v(bpy) ring-stretching vibrations were observed in the region 1400–1500 cm^{-1}, and were indicative of the localised oxidation-state distribution. This contrasts the situation in the structurally-related Class II system bridged by 4,4′-bpy in which the v(bpy) vibrations are an *average* of those in the Os^{II}Os^{II} and Os^{III}Os^{III} spectra.[12] While the v(bpy) and v(pyz) spectator vibrations provide useful oxidation state markers, they are only weakly-coupled to the electron transfer and provide a minimal contribution to the barrier.

One of the most comprehensive sets of experimental data for the transition between the localised and delocalised regimes has been observed by variation of the peripheral ligands in the series of the Creutz–Taube ion derivatives, *trans*-[{Ru(NH$_3$)$_5$}(μ-pyz){Ru(NH$_3$)$_4$(L)}]$^{5+}$ {L = NH$_3$, py (pyridine), 3,5-Me$_2$py (3,5-dimethylpyridine), 3-Cl-py (3-chloropyridine), 2,6-Me$_2$pyz (2,6-dimethylpyrazine)}[34c] illustrated in Fig. 8(a). As shown by Curtis and coworkers, the introduction of redox asymmetry (ΔE_0) by the incorporation of increasingly stronger back-bonding ligands results in a broadening and blue-shifting of the IVCT band.
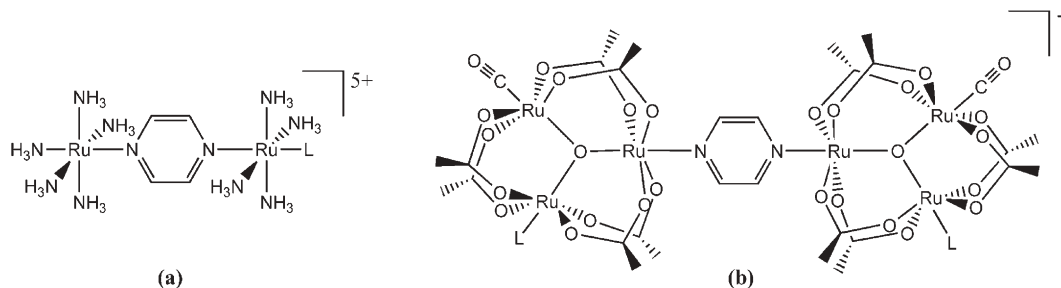
Fig. 8 (a) *Trans*-[{Ru(NH$_3$)$_5$}(μ-pyz){Ru(NH$_3$)$_4$(L)}]$^{5+}$ (L = py, 3,5-Me$_2$py, 3-Cl-py, 2,6-Me$_2$pyz).[34c] (b) Pyrazine-bridged clusters [{Ru$_3$(μ$_3$-O)(μ-O$_2$CCH$_3$)$_6$(CO)(L)}$_2$(μ-pyz)]$^-$ {L = 4-(dimethylamino)pyridine, pyridine, 4-cyanopyridine}.[26]

This journal is © The Royal Society of Chemistry 2006

Chem. Soc. Rev., 2006, **35**, 424–440 | 437

Kubiak and coworkers have investigated the IR line broadening and coalescence behaviour due to the dynamic coupling of the ν(CO) "spectator vibrations" to electron transfer in the pyrazine-bridged mixed-valence clusters $[\{Ru_3(\mu_3\text{-}O)(\mu\text{-}O_2CCH_3)_6(CO)(L)\}_2(\mu\text{-pyz})]^-$ {L = 4-(dimethyl-amino)pyridine, pyridine, 4-cyanopyridine} shown in Fig. 8(b).[26,36] Varying L through the series 4-(dimethyl-amino)pyridine, pyridine and 4-cyanopyridine results in an increase in H_{ab} and a change in the pattern of CO stretching vibrations from two discrete bands to a single averaged band. This is suggestive of increasing solvent averaging and demonstrates that the rate constant for electron transfer is determined by the solvent reorganisation frequency within the Class II–III regime.[26,36]

The complexity of factors which influence intramolecular electron transfer in the shift between the localised and delocalised regimes underlie the importance of *systematic* experimental studies of mixed-valence complexes in this region. However, a limited number of studies exist in which the subtleties in behaviour in this transition have been explored.[8,12–14,23] Consequently, there is extensive interest in the preparation of systems to guide and test the development of a unifying theory of electron transfer.[8,11,12]

Recently, Keene and coworkers have demonstrated that the diastereoisomers of symmetrical dinuclear mixed-valence complexes of ruthenium and osmium, *meso-* and *rac-* $[\{M(bpy)_2\}_2(\mu\text{-BL})]^{5+}$ (M = Ru, Os; BL = a series of di-bidentate polypyridyl bridging ligands such as 2,2′-bipyrimidine) provide subtle and systematic probes to examine the microscopic origins of the factors which govern the electron transfer barrier in eqn (1). The *meso* and *rac* diastereoisomeric forms differ only in terms of the relative orientations of the terminal ligands which give rise to different dimensions in the clefts formed between the bpy ligands immediately above and below the plane of the bridging ligand.[37] Within the classical framework, the λ_i and $\Delta E'$ contributions in eqn (1) are expected to be identical for both diastereoisomers, and since ΔE_0 is zero, the differential solvent dependencies of the IVCT bands for the two forms revealed that stereochemically-directed specific solvent effects dominated the continuum contribution to λ_o in eqn (11). The results also challenged prior assertions that the inherent stereochemical identity of such complexes would have no influence on the intramolecular electron transfer properties of polymetallic assemblies.

6. Issues for the spectral analysis of IVCT transitions

For systems in the localised-to-delocalised regime, the IVCT bands are frequently asymmetrically-shaped.[12–14] The two-state classical model attributes the asymmetry to the band cut-off effect; however the asymmetry may also arise due to overlapping IVCT and/or IC bands, differences in the extent of electronic delocalisation between the ground and mixed-valence excited states or contributions from vibronic progressions.[12–14] While the application of vibronic coupling theories with the inclusion of symmetric and anti-symmetric mode contributions is necessary for the band-shape analysis of

mixed-valence systems in the localised-to-delocalised regime, the classical analysis may be adequate if the widths of the separate vibronic components exceed their vibrational separation.

The majority of IVCT studies to date have focused on the comparison of the "raw" parameters of the IVCT bands (*i.e.* ν_{max}, ε_{max} and $\Delta\nu_{1/2}$); however, meaningful comparisons between the IVCT properties of mixed-valence complexes require the explicit consideration of the following factors:

(i) Since wavelength-dependent charge transfer intensities scale with the inverse of the absolute absorption energy (ν^{-1}),[1a] plots of ε/ν versus ν are expected to exhibit a Gaussian shape rather than plots of ε versus ν. The energy maximum of the "reduced" absorption spectrum (*i.e.* ε/ν versus ν) is identified with the vertical upper-/lower-surface energy separation and is the quantity most appropriately employed analysis of IVCT bands.

(ii) Due to comproportionation of the mixed-valence species, the proportion of the complex in the mixed-valence form (at equilibrium) is $K_c^{1/2}/(2 + K_c^{1/2})$, which must be accounted for in spectral analyses.

(iii) Deconvolutions of the mixed-valence spectra are required to account for the multiple IVCT and IC transitions which arise from spin–orbit coupling and ligand-field asymmetry; identification of the first component of the IVCT manifold is paramount, as this transition characterises the ground-state of the mixed-valence chromophore.[12]

(iv) Hush and Reimers[23] have highlighted the importance of the calculation of the moments of the IVCT bands {eqn (26)}, although this aspect appears not to have been generally appreciated by experimentalists.[11] Such analyses are particularly crucial for the elucidation of trends in the electronic coupling, solvatochromism and thermochromism properties of mixed-valence systems between the fully localised and delocalised regimes, where the asymmetric shapes of the bands frequently preclude the accurate determination of the component spin–orbit transitions. The zeroth-moment (M_0) represents the area under the band of the reduced absorption spectrum, where $f(\nu)$ is the line-shape function of the reduced absorption spectrum {(ε/ν) versus ν}. The transition moment ($|\mu_{12}|$ in eÅ) is defined as 0.0206 Å $\times$ $M_0^{1/2}$. The average energy of the absorption manifold is given by the first-order moment (M_1) and the second-order moment (M_2) measures of the standard deviation of the bands. The latter may serve as a more appropriate measure of the trends in the line-widths for asymmetrically-shaped bands and may assist in clarifying the contribution of symmetric modes to IVCT broadening in the localised-to-delocalised and delocalised regimes.

$$M_0 = \int_{\nu_1}^{\nu_2} f(\nu)d\nu, \; M_1 = \frac{1}{M_0}\int_{\nu_1}^{\nu_2} \nu f(\nu)d\nu$$
$$\text{and } M_2 = \frac{1}{M_0}\int_{\nu_1}^{\nu_2} \nu^2 f(\nu)d\nu - M_1^2$$

(26)

7. Conclusions and future challenges

Experimental studies of IVCT in dinuclear mixed-valence complexes have provided crucial insights into the fundamental factors that govern electronic delocalisation and the activation barriers to electron transfer, through the seminal theoretical

formalism pioneered by Hush.[1] Systems of this genre have provided important experimental insights into the roles of *intra-* and *intermolecular* contributions to IVCT, and they have been used as model systems to verify the salient predictions of several important theoretical models that describe the activation barriers.[4,5,8,14] Experimentally, contributions to the IVCT energy in eqn (1) arise from environmental contributions such as ion-pairing, solvation and the temperature of the medium, as well as intramolecular contributions due to structural factors which are dependent on the identity and coordination environments of the component metal centres.[4–12] In a number of cases, the theoretical analysis and implications of the results have been complicated by ion-pairing and specific solvation effects, as well as ambiguities in the geometries of the complexes due to a lack of structural rigidity and/or stereoisomeric purity. For example, complexes incorporating non-rigid bridging ligands pose an additional complexity, as the inherent structural distortion introduces an effective redox asymmetry contribution.[37]

Over the past decade, significant interest has been directed towards the observation of microscopic contributions to the IVCT properties in order to develop more sophisticated theoretical and computational models for the fundamental factors that contribute to the electron transfer barrier. For example, intermolecular effects such as specific solvent interactions have been shown to provide a significant contribution to the IVCT energy, which may dominate continuum contributions.[11] Continuing investigations of the differential IVCT characteristics in the diastereoisomeric forms of dinuclear polypyridyl complexes of ruthenium and osmium provide an interesting means of probing spatial contributions to intramolecular electron transfer at the molecular level.[37a,b]

The observation of microscopic contributions to the electron transfer barrier, such as stereochemically-directed solvent and anion interactions, may assist in unravelling the intricate factors which govern the structure–function relationship in biological systems. At an applied level, such molecular-scale effects could ultimately be exploited in the rational design of higher-nuclearity assemblies which form the basis of novel molecular materials.

While the majority of IVCT analyses are based primarily on a semi-classical two-state analysis for IVCT, a minimum of three-states is required to adequately account for the integral role of the bridging ligands in mediating the IVCT process *via* a superexchange mechanism. In this case, the trends in the IVCT properties are more accurately analysed on the basis of a qualitative three-state model which includes the influence of the symmetric vibration mode. Often, the accurate quantitative treatment of the results requires consideration of the full vibronic coupling problem, with the inclusion of *both* symmetric and anti-symmetric vibration modes. The recent success of such treatments in modelling the mixed-valence special-pair radical cation of the photosynthetic reaction centre is encouraging in this regard,[29] and there is significant potential for the application of these methods to dinuclear mixed-valence systems.

For the completely delocalised mixed-valence systems, the symmetric mode contributions dictate the IVCT lineshape in the delocalised limit and studies of ion-pairing and polarisability effects within this regime represent an important avenue of future research. Indeed, the systematic investigation of the factors influencing IVCT in delocalised mixed-valence systems has received limited attention compared with studies of localised systems.

In parallel with analyses of the IVCT absorption bands, an important thrust of future research involves the measurement of IR and resonance Raman spectra which quantify mode-specific contributions to the electron transfer barrier. As detailed by Meyer and coworkers, the appearance and relative intensities of symmetrical bridging ligand stretches and the extent of averaging of the terminal ligand vibrations in the IR region provide one of the most definitive means for assessing the relative degree of electronic delocalisation, and distinguishing between the localised and delocalised regimes.[12] In addition, the experimental data will provide an extensive platform for testing existing vibronic coupling theories for IVCT (such as the PKS model[24] and the vibronic coupling model of Reimers and Hush[23]) and guiding developing theories which explicitly include symmetric vibration modes.[23]

A further important avenue of research is the consideration of more sophisticated models for the treatment of IVCT electroabsorption (Stark effect) data, as the classical two-state Liptay analysis is inappropriate for the treatment of systems in the localised-to-delocalised regime. Boxer and coworkers[38] have recently postulated a general theoretical formalism to treat moderately- to strongly-coupled mixed-valence systems, and there is a need for detailed tests of the applicability of such treatments for systems in the intermediate region.

In this review we have sought to highlight the complexity of factors that require consideration in the analysis of IVCT transitions. A particular aspect that requires emphasis is the need for standard conditions of solvent, electrolyte and temperature to enable meaningful comparisons between the results from IVCT studies. We hope that the clarification of these issues will motivate systematic experimental studies to probe the transition between localisation and delocalisation which will guide the development of theoretical models for the intermediate regime which are parameterised in terms of physically-transparent quantities.

Acknowledgements

References

1 (*a*) N. S. Hush, *Prog. Inorg. Chem.*, 1967, **8**, 391; (*b*) N. S. Hush, *Electrochim. Acta*, 1968, **13**, 1005.
2 J. T. Hupp, in *Comprehensive Coordination Chemistry II*, ed. T. J. Meyer and J. A. McCleverty, Elsevier, Oxford, 2004, vol. 2, pp. 709–717; and references therein.
3 M. B. Robin and P. Day, *Adv. Inorg. Chem. Radiochem.*, 1967, **10**, 247.

This journal is © The Royal Society of Chemistry 2006

Chem. Soc. Rev., 2006, **35**, 424–440 | 439

4 C. Creutz, *Prog. Inorg. Chem.*, 1983, **30**, 1.
5 R. J. Crutchley, *Adv. Inorg. Chem.*, 1994, **41**, 273.
6 K. Kalyanasundaram and M. K. Nazeeruddin, *Inorg. Chim. Acta*, 1994, **226**, 213.
7 M. D. Ward, *Chem. Soc. Rev.*, 1995, **24**, 121.
8 P. F. Barbara, T. J. Meyer and M. A. Ratner, *J. Phys. Chem.*, 1996, **100**, 13148.
9 J.-P. Launay, *Chem. Soc. Rev.*, 2001, **30**, 386.
10 W. Kaim, A. Klein and M. Glöckle, *Acc. Chem. Res.*, 2000, **33**, 755.
11 P. Chen and T. J. Meyer, *Chem. Rev.*, 1998, **98**, 1439.
12 K. D. Demadis, C. M. Hartshorn and T. J. Meyer, *Chem. Rev.*, 2001, **101**, 2655.
13 S. F. Nelsen, *Chem.–Eur. J.*, 2000, **6**, 581.
14 B. S. Brunschwig, C. Creutz and N. Sutin, *Chem. Soc. Rev.*, 2002, **31**, 168.
15 B. S. Brunschwig and N. Sutin, *Coord. Chem. Rev.*, 1999, **187**, 233.
16 For low frequency modes, $\omega \ll k_B T$, where $k_B T \sim 200$ cm^{-1} at room temperature and $\omega \sim 1$–10cm^{-1} for polar solvents. For high-frequency modes, $\omega \gg k_B T$. , ω and k_B denote Planck's constant, the vibrational frequency and Boltzmann's constant, respectively.
17 J. T. Hupp and R. D. Williams, *Acc. Chem. Res.*, 2001, **34**, 808.
18 C. Creutz, M. D. Newton and N. Sutin, *J. Photochem.*, 1994, **82**, 47.
19 D. E. Richardson and H. Taube, *Coord. Chem. Rev.*, 1984, **60**, 107.
20 G. Giuffrida and S. Campagna, *Coord. Chem. Rev.*, 1994, **135**, 517.
21 G. M. Sando, PhD thesis, Northwestern University, Evanston, IL, USA, 2003.
22 M. Al-Noaimi, G. P. A. Yap and R. J. Crutchley, *Inorg. Chem.*, 2004, **43**, 1773 and references therein.
23 J. R. Reimers and N. S. Hush, *Chem. Phys.*, 1996, **208**, 177.
24 (*a*) S. B. Piepho, E. R. Krausz and P. N. Schatz, *J. Am. Chem. Soc.*, 1978, **100**, 2996; (*b*) K. Y. Wong and P. N. Schatz, *Prog. Inorg. Chem.*, 1981, **28**, 369; (*c*) S. B. Piepho, *J. Am. Chem. Soc.*, 1990, **112**, 4197.
25 (*a*) M. J. Ondrechen, J. Ko and L. J. Root, *J. Phys. Chem.*, 1984, **88**, 5919; (*b*) J. Ko and M. J. Ondrechen, *J. Am. Chem. Soc.*, 1985, **107**, 6161; (*c*) A. Ferretti, A. Lami, M. J. Ondrechen and G. Villani, *J. Phys. Chem.*, 1995, **99**, 10484; (*d*) M. J. Ondrechen, J. Ko and L.-T. Zhang, *J. Am. Chem. Soc.*, 1987, **109**, 1672.
26 C. H. Londergan and C. P. Kubiak, *J. Phys. Chem. A*, 2003, **107**, 9301.
27 M. D. Newton, *Chem. Rev.*, 1991, **91**, 767.
28 (*a*) N. S. Hush and J. R. Reimers, *Coord. Chem. Rev.*, 1998, **177**, 37; (*b*) N. S. Hush and J. R. Reimers, *Chem. Rev.*, 2000, **100**, 775.
29 J. R. Reimers and N. S. Hush, *J. Am. Chem. Soc.*, 2004, **126**, 4123.
30 V. Balzani, A. Juris, M. Venturi, S. Campagna and S. Serroni, *Chem. Rev.*, 1996, **96**, 759.
31 (*a*) G. U. Bublitz and S. G. Boxer, *Annu. Rev. Phys. Chem.*, 1997, **48**, 213; (*b*) B. S. Brunschwig, C. Creutz and N. Sutin, *Coord. Chem. Rev.*, 1998, **177**, 61; (*c*) K. A. Walters, in *Comprehensive Coordination Chemistry II*, ed. T. J. Meyer and J. A. McCleverty, Elsevier, Oxford, 2004, vol. 2, pp. 303–313; (*d*) A. Ferretti, *Coord. Chem. Rev.*, 2003, **238–239**, 127; (*e*) F. W. Vance, R. D. Williams and J. T. Hupp, *Int. Rev. Phys. Chem.*, 1998, **17**, 307.
32 W. Liptay, *Angew. Chem., Int. Ed. Engl.*, 1969, **8**, 177.
33 J. R. Reimers and N. S. Hush, *J. Phys. Chem.*, 1991, **95**, 9773.
34 (*a*) J. C. Curtis, J. S. Bernstein, R. H. Schmehl and T. J. Meyer, *Chem. Phys. Lett.*, 1981, **81**, 48; (*b*) F. Salaymeh, S. Berhane, R. Yusof, R. Delarosa, E. Y. Fung, R. Matamoros, K. W. Lau, Q. Zheng, E. M. Kober and J. C. Curtis, *Inorg. Chem.*, 1993, **32**, 3895; (*c*) R. de la Rossa, P. J. Chang, F. Salaymeh and J. C. Curtis, *Inorg. Chem.*, 1985, **24**, 4229; (*d*) X. L. Zhang, D. I. Yoon and J. T. Hupp, *Inorg. Chim. Acta*, 1995, **240**, 285.
35 P. H. Dinolfo, S. J. Lee, V. Coropceanu, J.-L. Brédas and J. T. Hupp, *Inorg. Chem.*, 2005, **44**, 5789.
36 J. C. Salsman, C. P. Kubiak and T. Ito, *J. Am. Chem. Soc.*, 2005, **127**, 2382.
37 (*a*) D. M. D'Alessandro and F. R. Keene, *Chem. Phys.*, 2006, DOI: 10.1016/j.chemphys.2005.09.016 in the press; (*b*) D. M. D'Alessandro, L. S. Kelso and F. R. Keene, *Inorg. Chem.*, 2001, **40**, 6841; (*c*) D. M. D'Alessandro, P. C. Junk and F. R. Keene, *Supramol. Chem.*, 2005, **17**, 529–542.
38 T. P. Treynor and S. G. Boxer, *J. Phys. Chem. A*, 2004, **108**, 1764.